group. This would contribute to increased differentiation of recruited osteogenic cells to osteoblasts and subsequently enhanced osteogenesis in the defect from day 14 to day 21. It is speculated that released simvastatin from resorbing αTCP stimulated the BMP-2 expression of osteogenic cells that were migrated from the dura mater and recruited around and inside αTCP particles at day 3. At later time points, auto- and paracrine upregulation of BMP-2 would play a role in continuing osteoblast differentiation and osteogenesis.

Maeda et al reported that statins augment vascular endothelial growth factor (VEGF) in osteoblastic cells *in vitro*.[32] In this animal study, VEGF was upregulated from day 7 to day 21 although the expression was not statistically different from control and TCP groups. Histologically, all groups revealed similar patterns of angiogenesis in the defect region.

Certain conditions must be considered when selecting an appropriate carrier or delivery system for drugs : (1) the ability of the system to deliver the drug at the appropriate time and in the proper dose, (2) the presence of a substratum that will enhance cell recruitment and attachment and will potentiate chemotaxis, (3) the presence of a void space to allow for cell migration and to promote angiogenesis, and (4) the ability of the delivery system to biodegrade without generating an immune or inflammatory response and without producing toxic waste products that would inhibit the repair process.[33] Alpha TCP used in this study fulfils all these requirements as a proper drug delivery system. It could release simvastatin sufficiently at the early time point when there is increased cellular proliferation and recruitment, thus augmenting the proliferation and recruitment of osteoprogenitor cells during this phase. Histological findings show that αTCP particles provided spaces into which osteogenic cells migrated and recruited. The particles also maintained spaces between them so that migrating osteogenic cells could be recruited and consequently differentiated and formed new bone whereas in control defects, middle of the bone defect was occupied by the connective tissue. Moreover, gradual dissolution of αTCP allowed a smooth exchange with newly formed bone without causing inflammatory response.

Although real-time PCR analysis indicated enhanced upregulation of BMP-2 and TGF-β1 mRNA expressions in simvastatin-αTCP combination group, it is not clear in which particular cell types these gene expressions were upregulated. Further studies using in-situ hybridization to detect the location of mRNAs would provide more information regarding the possible stimulatory effects of simvastatin on various cells in the bone defect. In addition, experiments to explore changes in the expression of other important genes such as FGF-2 and PDGF, which are also known to support cellular migration and proliferation, are also necessary for better understanding of the multiple effects of simvastatin in the molecular pathways that are involved in bone healing process.

In conclusion, within the limitation of this study, simvastatin combined with alpha tricalcium phosphate induced bone regeneration in rat calvarial defects by augmenting osteogenic cell proliferation, migration, recruitment and differentiation in the early phase of bone healing which were associated with increased expression of BMP-2 and TGF-β1.

REFERENCES

1. Einhorn TA. Clinical applications of recombinant human BMPs: Early experience and future development. J Bone Joint Surg Am 2003;85:82–88.
2. Mundy G, Garrett R, Harris S, Chan J, Chen D, Rossini G, Boyce B, Zhao M, Gutierrez G. Stimulation of bone formation in vitro and in rodents by statins. Science 1999;18:53–57.
3. Thylin MR, McConnell JC, Schmid MJ, Reckling RR, Ojha J, Bhattacharyya I, Marx DV, Reinhardt RA. Effects of statin gels on murine calvarial bone. J Periodontol 2002;73:1141–1148.
4. Wong RWK, Rabie ABM. Statin collagen grafts used to repair bone defects in the parietal bone of rabbits. Br J Oral Maxillofac Surg 2003;41:244–248.
5. Stein D, Lee Y, Schmid MJ, Killpack B, Genrich MA, Narayana N, Mark DB, Cullen DM, Reinhardt RA. Local simvastatin effects on mandibular bone growth and inflammation. J Periodontol 2005;76:1861–1870.
6. Sato D, Nishimura K, Ishioka T, Kondo H, Kuroda S, Kasugai S. Local application of simvastatin to rat incisor socket: Carrier-dependent effect on bone augmentation. J Oral Tissue Eng 2005;2:81–85.
7. Nyan M, Sato D, Oda M, Machida T, Kobayashi H, Nakamura T, Kasugai S. Bone formation with the combination of simvastatin and calcium sulfate in critical-sized rat calvarial defect. J Pharmacol Sci 2007;104:384–386.
8. Garrett IR, Gutierrez GE, Rossini G, Nyman J, McCluskey B, Flores A, Mundy GR. Locally delivered lovastatin nanoparticles enhance fracture healing in rats. J Orthop Res 2007;25:1351–1357.
9. Ozec I, Kilic E, Gumus C, Goze F. Effect of local simvastatin application on mandibular defects. J Craniofac Surg 2007;18:546–550.
10. Wang JW, Xu SW, Yang DS, Lv RK. Locally applied simvastatin promotes fracture healing in ovariectomized rat. Osteoporos Int 2007;18:1641–1650.
11. Wu Z, Liu C, Zang G, Sun H. The effect of simvastatin on remodeling of the alveolar bone following tooth extraction. Int J Oral Maxillofac Surg 2008;37:170–176.
12. Lee Y, Schmid MJ, Marx DB, Beatty MW, Cullen DM, Collins ME, Reinhardt RA. The effect of local simvastatin delivery strategies on mandibular bone formation in vivo. Biomaterials 2008;29:1940–1949.
13. Ma B, Clarke SA, Brooks RA, Rushton N. The effect of simvastatin on bone formation and ceramic resorption in a periimplant defect model. Acta Biomater 2008;4:149–155.
14. Moriyama Y, Ayukawa Y, Ogino Y, Atsuta I, Koyano K. Topical application of statin affects bone healing around implants. Clin Oral Impl Res 2008;19:600–605.
15. Jeon JH, Piepgrass WT, Lin YL, Thomas MV, Puleo DA. Localized intermittent delivery of simvastatin hydroxyacid stimulates bone formation in rats. J Periodontol 2008;79:1457–1464.
16. Ayukawa Y, Yasukawa E, Moriyama Y, Ogino Y, Wada H, Atsuta I, Koyano K. Local application of statin promotes

bone repair through the suppression of osteoclasts and the enhancement of osteoblasts at bone-healing sites in rats. Oral Surg Oral Med Oral Pathol Oral Radiol Endod 2008;107:336–342.
17. Nyan M, Sato D, Kihara H, Machida T, Ohya K, Kasugai S. Effects of the combination with alpha-tricalcium phosphate and simvastatin on bone regeneration. Clin Oral Impl Res 2009;20:280–287.
18. Einhorn TA. The cell and molecular biology of fracture healing. Clin Orthop 1998;355S:7–21.
19. Gerstenfeld LC, Cullinane DM, Barnes GL, Graves DT, Einhorn TA. Fracture healing as a post-natal developmental process: Molecular, spatial, and temporal aspects of its regulation. J Cell Biochem 2003;88:873–84.
20. Hobar PC, Masson JA, Wilson R, Zerwekh J. The importance of the dura in craniofacial surgery. Plast Reconstr Surg 1996;98:217–225.
21. Drake DB, Persing JA, Berman DE, Ogle RC. Calvarial deformity regeneration following subtotal craniectomy for craniosynostosis: A case report and theoretical implications. J Craniofac Surg 1993;4:85–89.
22. Opperman LA, Sweeney TM, Redmon J, Persing JA, Ogle RC. Tissue interactions with underlying dura mater inhibit osseous obliteration of developing cranial sutures. Dev Dyn 1993;198:312–322.
23. Gosain AK, Santoro TD, Song LS, Capel CC, Sudhakar PV, Madoub HS. Osteogenesis in calvarial defects: Contribution of the dura, the pericranium, and the surrounding bone in adult versus infant animals. Plast Reconstr Surg 2003;112: 515–527.
24. Ogle RC, Tholpady SS, McGlynn KA, Ogle RA. Regulation of cranial suture morphogenesis. Cells Tissues Organs 2004; 176:54–66.
25. Lind M, Eriksen EF, Bünger C. Bone morphogenetic protein-2 but not bone morphogenetic protein-4 and-6 stimulates chemotactic migration of human osteoblasts, human marrow osteoblasts, and U2-OS cells. Bone 1996;18:53–57.
26. Fiedler J, Röderer G, Günther KP, Brenner RE. BMP-2. BMP-4, and PDGF-bb stimulate chemotactic migration of primary human mesenchymal progenitor cells. J Cell Biochem 2002;87:305–12.
27. Lieberman JR, Daluiski A, Einhorn TA The role of growth factors in the repair of bone: Biology and clinical applications. J Bone Joint Surg Am 2002;84:1032–1044.
28. Marcelli C, Yates AJP, Mundy GR. In vivo effects of human recombinant transforming growth factor beta on bone turnover in normal mice. J Bone Miner Res 1990;5:1087–1096.
29. Noda M, Camilliere JJ. In vivo stimulation of bone formation by transforming growth factor-beta. Endocrinology 1989;124: 2991–2994.
30. Lind M. Growth factor stimulation of bone healing. Effects on osteoblasts, osteotomies, and implants fixation. Acta Orthop Scand Suppl 1998;83:2–37.
31. Bruder SP, Fink DJ, Calpan AI. Mesenchymal stem cells in bone development, repair, and skeletal regeneration therapy. J Cell Biochem 1994;56:283–294.
32. Maeda T, Kawabe T, Horiuchi N. Statins augment vascular endothelial growth factor expression in osteoblastic cells via inhibition of protein prenylation. Endocrinology 2003;144: 681–692.
33. Lieberman JR, Daluiski A, Stevenson S, Wu L, McAllister P, Lee YP, Kabo JM, Finerman GA, Berk AJ, Witte ON. The effect of regional gene therapy with bone morphogenetic protein-2-producing bone-marrow cells on the repair of segmental femoral defects in rats. J Bone Joint Surg Am 1999;81: 905–917.

CLINICAL ORAL IMPLANTS RESEARCH

Kazuhiro Kon
Makoto Shiota
Maho Ozeki
Yasuo Yamashita
Shohei Kasugai

Bone augmentation ability of autogenous bone graft particles with different sizes: a histological and micro-computed tomography study

Authors' affiliations:
Kazuhiro Kon, Makoto Shiota, Maho Ozeki, Shohei Kasugai, Department of Oral Implantology and Regenerative Dental Medicine, Tokyo Medical and Dental University, Bunkyo-ku, Tokyo, Japan
Yasuo Yamashita, Department of Maxillofacial Anatomy, Tokyo Medical and Dental University, Bunkyo-ku, Tokyo, Japan

Correspondence to:
Kazuhiro Kon
Department of Oral Implantology and Regenerative Dental Medicine
Tokyo Medical and Dental University
1-5-45 Yushima
Bunkyo-ku
Tokyo 113-8549
Japan
Tel./Fax: +81 3 5803 5774
e-mail: k-kon.irm@tmd.ac.jp

Date:
Accepted 26 May 2009

To cite this article:
Kon K, Shiota M, Ozeki M, Yamashita Y, Kasugai S. Bone augmentation ability of autogenous bone graft particles with different sizes: a histological and micro-computed tomography study.
Clin. Oral Impl. Res. 20, 2009; 1240–1246.
doi: 10.1111/j.1600-0501.2009.01798.x

Key words: bone graft, dental implant, histology, micro-CT analysis

Abstract

Objectives: The purpose of this study was to investigate the augmentation process and ability of autogenous bone graft particles of two different sizes in a vertical augmentation chamber.

Material and methods: The cranial bones of 24 rabbits were used. Two polytetrafluoroethylene chambers were filled with harvested bone from tibia with small bone (SB; 150–400 μm) and large bone (LB; 1.0–2.0 mm) of the same weight. Animals were sacrificed after 1, 2, 4 and 8 weeks. The samples were analyzed by micro-computed tomography (micro-CT) for quantitative analysis, and embedded in polyester resin as non-decalcified specimens for histological analysis. Total bone volume (TBV), bone height (BH) and distribution of bone structure were calculated by micro-CT.

Results: Micro-CT evaluation and histology revealed a significant difference between the investigated specimens. TBV and BH of SB decreased to about 50% of the initial situation, and there was a statistically significant difference between 1 and 8 weeks. In contrast, TBV and BH of LB were almost retained at all experimental time points. Significant differences in TBV and BH were also observed between LB and SB at 8 weeks. Bone volume of SB decreased predominantly in the upper half of the chamber at 4 and 8 weeks. In the histological observations, SB showed favorable new bone formation and rapid bone resorption in a time-dependent manner during the entire experimental period. However, LB exhibited favorable morphological stability and continued new bone formation.

Conclusion: SB follows a smooth osteogenic process, whereas it is not effective in volume augmentation. LB is superior to SB in augmentation ability.

Oral implant therapy is now widely accepted as it provides a satisfactory esthetic and functional outcome (Ferrigno et al. 2002; Boronat-Lopez et al. 2009). To achieve these results, edentulous jaws should have adequate bone volume, which enables the placement of implants in an ideal position. In many cases, implant placement was restricted by bone resorption after teeth extraction, or the position of the mandibular canal and maxillary sinus. Therefore, bone augmentation is frequently planned in association with implant therapy (Lustmann & Lewinstein 1995; Chiapasco et al. 2004; Fugazzotto & Vlassis 2007; Hämmerle et al. 2008).

Currently, autogenous bone, allogeneic bone, xenogeneic bone and synthetic bone are being used as bone grafting materials (Moy et al. 1993; Yildirim et al. 2000; Rodriguez et al. 2003; Scabbia & Trombelli 2004; Turunen et al. 2004; Kihara et al. 2006). Among them, autogenous bone is widely regarded as the gold standard (Boyne

& James 1980; Moy et al. 1993). However, autogenous bone grafts have several disadvantages, including morbidity of the donor site, limited amount of harvestable bone and ongoing volume reduction during the healing period. Especially, many researchers have demonstrated resorption of the grafted autogenous bone after surgery. Clinically, reduction of the buccal tissue volume was observed after autogenous block bone grafting in long-term follow-up studies (Widmark et al. 1997; Jemt & Lekholm 2003). The authors described this phenomenon as the result of grafted bone resorption. Moreover, autogenous bone grafted for maxillary sinus augmentation was reduced 6 months after surgery (Johansson et al. 2001).

The particle size of autogenous bone, which is considered to be one of the important factors that determine the augmentation ability, was studied in some articles (Zaner & Yukna 1984; Fucini et al. 1993; Springer et al. 2004; Murai et al. 2006; Coradazzi et al. 2007; Kuroki et al. 2008; Walsh et al. 2008). However, the conclusions of these investigations varied.

The purpose of this study was to investigate the augmentation process of autogenous bone graft particles of two different sizes in a vertical augmentation chamber and evaluate their augmentation ability.

Material and methods

Experimental protocols were approved by the Institutional Committee of Animal Care and Use at Tokyo Medical and Dental University. Japanese male white rabbits of weight (3.2–3.8 kg) and size were used (n = 24).

Surgical procedures

Animals were anesthetized preoperatively with an intramuscular injection of ketamine (50 mg/kg Ketalar, Sankyo, Tokyo, Japan) and thiopental sodium (25 mg/kg Rabonal, Tanabe, Tokyo, Japan). The surgical area was shaved and disinfected. In addition, 1.8 ml of a local anesthetic (2% xylocaine/epinephrine 1 : 80,000, Dentsply Sankin, Tokyo, Japan) was injected into the surgical sites before the start of surgery. Autogenous bone particles of two sizes were harvested from the tibia. The large particle bone (LB), which was cuboidal in shape (about 1 mm thickness and width with 2 mm length, standardized by sieves), was harvested with bone forceps. The small particle bone (SB), which was bone debris (150–400 μm diameter, average 250 μm), was harvested by a 3.2-mm-diameter trephine-bone-mill system (K-System, DentaK, Paris, France). Parietal bone was chosen as the augmentation model site. Skin incision and subperiosteal dissection were carried out sagittally between the parietal and the frontal bone, and the periosteum was raised. Polytetrafluoroethylene chambers (hollow cylinders with 5.0 mm inner diameter and 3.0 mm height having an outer brim) were fixed with stainless-steel screws (FKG Dentaire, Chaux-de-Fonds, Switzerland) to the parietal bone on the right and left sides. Bone of the same weight (60 mg) was grafted into each chamber with peripheral blood. The skin flaps were sutured with 3-0 silk. During the observation period, all rabbits were given water and a standard rabbit feed *ad libitum*. Rabbits were sacrificed at 1 week ($n = 6$), 2 weeks ($n = 6$), 4 weeks ($n = 6$) and 8 weeks ($n = 6$) with a lethal dose of thiopental sodium. The entire cranial bone was removed and fixed for 10 days in neutral 10% formalin.

Micro-computed tomography (micro-CT) analysis

Following the fixation period, grafted regions of specimens were quantified via micro-CT analysis (SMX-90CT, Shimadzu, Kyoto, Japan). Total bone volume (TBV) and bone height (BH) were calculated. TBV was acquired by the radiopaque voxels (cube 60 μm on one side) observed in the chamber. BH was evaluated from the distance between the basal host bone and the highest point of the bone fragment in the chamber and was measured in the center 3.0 mm diameter part of the chamber in each animal. The bone volume distribution in the upper and lower halves was also described as a percentile.

Histological processing

To obtain non-decalcified sections, cranial bone ($n = 24$) was dehydrated in ascending grades of ethanol, following fixation, and then embedded in polyester resin (Rigolac-70F, Rigolac-2004, Nisshin EM Co., Tokyo, Japan). These sections were cut (Exakt, Mesmer, Ost Einbeck, Germany) in the sagittal direction and ground to a thickness of about 300 μm. The sections were finally stained with 0.1% toluidine blue. Histological observation was performed under a light microscope.

Statistical analysis

To evaluate the influence of particle size on TBV and BH, intergroup data at each time point were statistically compared using the Kruskal–Wallis test and nonparametric multiple comparisons by Dunnet T3. Particle comparison within the same time point was analyzed using the Mann–Whitney test. *P*-values lt;0.05 were considered statistically significant. All statistical analyses were performed using a commercial computer program (SPSS 11.5, SPSS Inc., Chicago, IL, USA).

Results

Histology

SB-grafted sites

1 week. SB densely occupied almost the entire augmentation chamber and blood cells filled the inter-SB space. SB, which stained strongly with toluidine blue, retained its original chip-like shape. No osteoclast- or osteoblast-like cells were observed at this stage (Fig. 1a and b).

2 weeks. SB occupied nearly entire the chamber as in the first week, and the height of SB did not change (Fig. 2a). At the lower part of the chamber, numerous multinuclear giant cells were observed on the surface of SB, newly formed bone was partially observed on the surface of grafted bone and large amounts of fibrous connective tissue were observed in the interspace of the graft. Especially, in the region close to host bone, new blood vessels had formed. However, at the upper part of the chamber, there was no new bone formation; instead, part of the SB had undergone resorption by multi nuclear giant cells (Fig. 2c).

4 weeks. Bone area that exhibited constricted bone trabeculae occupied about half or more of the height of the chamber. Grafted SB had resorbed mostly in the upper part (Fig. 3a). Loose fibrous connective tissue was observed in the upper half of the chamber, and some fibrous connective tissue ran in a direction parallel to the bone

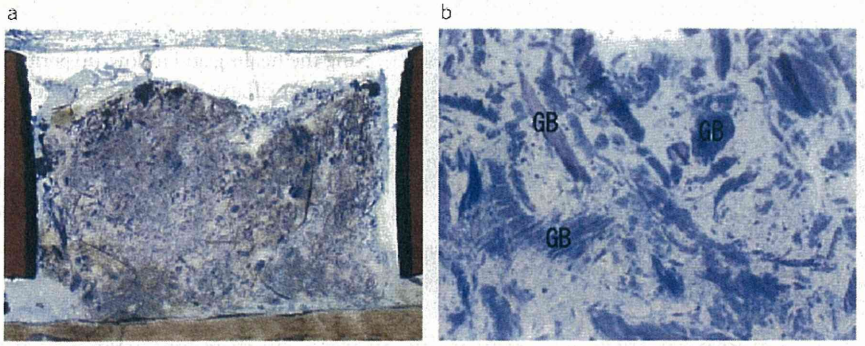

Fig. 1. Small bone grafted site at 1 week. (a) Grafted bone (GB) was observed over the entire augmentation chamber. GB retained its original chip-like shape. However, no newly formed bone was observed. Magnification × 2.5. (b) High-magnification image of (a). GB was strongly stained with toluidine blue. The interparticular space was occupied by blood cells. Magnification × 50.

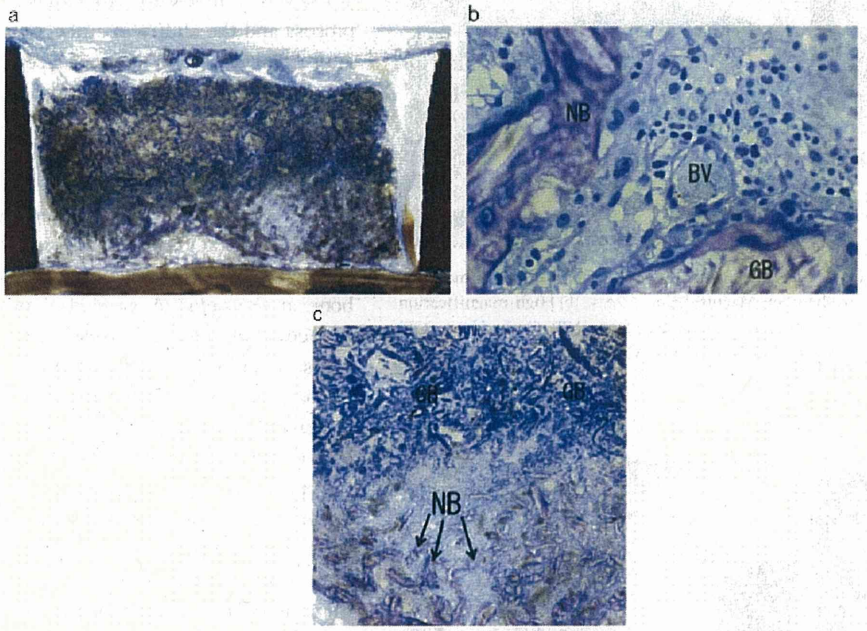

Fig. 2. Small bone grafted site at 2 weeks. (a) Grafted bone (GB) occupied the the entire chamber same as the 1-week model. The GB height was almost preserved. Magnification × 2.5. (b) High-magnification image of (a). New bone formation was observed from the region close to the host bone surface toward the GB. Blood vessels (BV) were also observed. Magnification × 100. (c) In the lower part of the chamber, near the host bone, newly formed bone (NB) was observed on the GB surface. In the upper part of the chamber, there was no new bone formation; instead, a part of GB underwent resorption by a multinuclear giant cell. Magnification × 10.

area. At higher magnification, grafted SB was mostly resorbed and replaced by newly formed bone. Mature blood vessels were observed in the interspace of the bone structure, and many fat cells were observed around the host bone (Fig. 3b).

8 weeks. The height of bone area was about a quarter of the chamber and the number of trabeculae had reduced when compared with the 4-week specimens. Loose fibrous connective tissue was observed in the upper region of the chamber. A large number of fat cells were observed over the entire chamber (Fig. 4a). Grafted bone was almost completely replaced by new bone that was surrounded by blood vessels and fat cells. Osteoclast-like cells were observed in the resorption lacunae within newly formed bone (Fig. 4b).

LB-graft sites

1 week. LB occupied a large part of the chamber. LB stained less with toluidine blue and resorption lacuna were not detected on the surface of grafted bone at this time point (Fig. 5a). In the interspace of grafted bone, very loose fibrous connective tissue and a few blood vessels were observed (Fig. 5b).

2 weeks. LB preserved its original block-like shape and low stainability. The height and space of the bone structure was maintained. The interspace of the grafted bone was filled with fibrous connective tissue (Fig. 6a). A few osteoclast-like cells were observed on the grafted bone. In the vicinity of the host bone, moderately mature blood vessels were found, and new bone had formed from the host bone surface toward the grafted bone (Fig. 6b).

4 weeks. LB was positioned at a higher level in the chamber and it retained its original form and low stainability (Fig. 7a). However, new bone formation was observed from the host bone surface to the grafted bone surface and Howship's lacunae with many osteoclast-like cells were found on the surface of the grafted bone in the upper part of the chamber (Fig. 7b). Fibrous connective tissue and blood vessels were observed around the grafted bone, and fat cells were detected around the host bone surface.

8 weeks. LB was only modestly integrated with newly formed bone that had high stainability, and the graft stained slightly stronger than at 4 weeks. Many osteocyte-like cells were observed on the grafted bone and a few osteoclast-like cells were also detected in the resorption lacunae (Fig. 8a). Around this bone architecture, numerous blood vessels were observed (Fig. 8b). There were many fat cells over the entire chamber, especially, near the host bone surface.

Micro-CT analysis

Radiological quantitative analysis was performed by micro-CT (Fig. 9)

Intergroup comparisons. TBV showed significant differences for 1 week/8 weeks in the SB group ($P = 0.026$), and 2/4 weeks in the LB group ($P = 0.025$). BH showed significant differences for 1 week/4 weeks ($P < 0.001$), 1 week/8 weeks ($P < 0.001$), 2/4 weeks ($P < 0.001$) and 2/8 weeks ($P < 0.001$) in the SB group. No other significant differences were found (Fig. 10a and b).

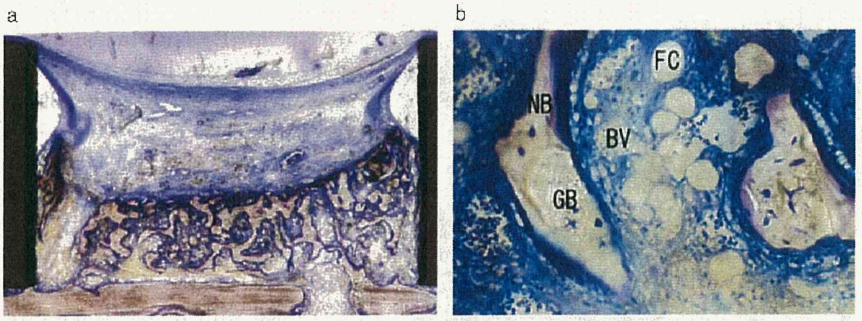

Fig. 3. Small bone grafted site at 4 weeks. (a) Newly formed bone (NB) occupied about half or more the height of the chamber. NB constricted bone trabeculae. Magnification × 2.5. (b) High-magnification image of (a). NB was observed around the grafted bone (GB). Mature blood vessels (BV) and fat cells (FC) were also observed in the interspace of the bone structure. Magnification × 50.

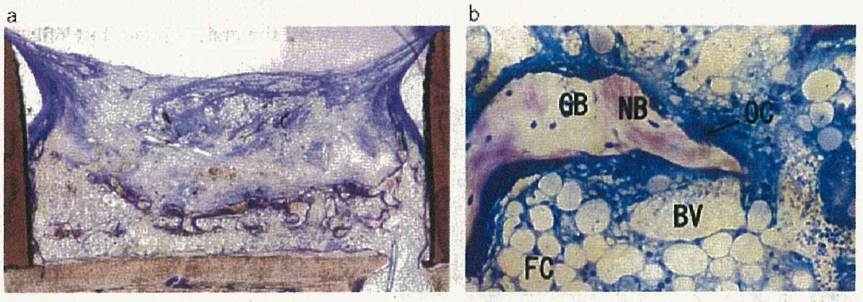

Fig. 4. Small bone grafted site at 8 weeks. (a) Accelerated bone resorption was observed in the 8-week model. A large number of fat cells were observed over the entire chamber. Magnification × 2.5. (b) High-magnification image of (a). Mature blood vessels (BV) were observed around the newly formed bone (NB). Grafted bone (GB) was almost completely replaced by new bone. An osteoclast-like cell (OC) was observed in the NB. Magnification × 100. FC, fat cell.

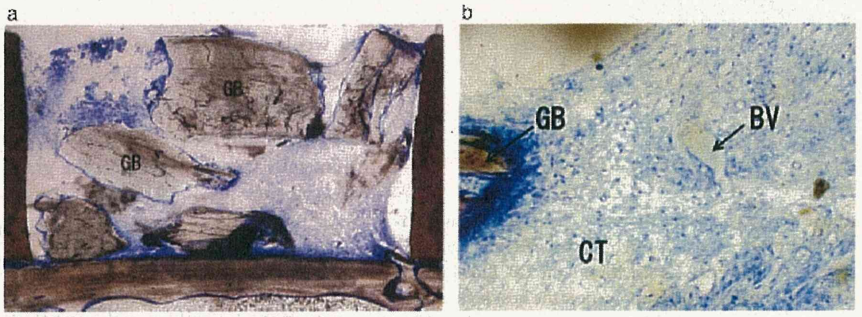

Fig. 5. Large bone grafted site at 1 week. (a) Grafted bone (GB) was observed over the entire chamber. Bone resorption was not observed around the surface of GB at this time point. Magnification × 2.5. (b) High-magnification image of (a). In the interspace of the GB, there was very loose fibrous connective tissue (CT), and a few blood vessels (BV) were also observed. Magnification × 25.

SB vs. LB

TBV and BH showed notable significant differences at 4 weeks (TBV: $P = 0.004$, BH: $P = 0.002$) and 8 weeks (TBV: $P = 0.006$, BH: $P = 0.004$). At 1 week and 2 weeks, there was no significant difference (Fig. 10a and b).

Distribution of bone structure

LB groups exhibited no remarkable changes. In contrast, bone volume reduction of the upper half was prominent in the 4- and 8-weeks of SB groups (Fig. 10c).

Discussion

Autogenous bone has long been considered the most excellent material for bone augmentation (Boyne & James 1980; Moy et al. 1993). However, it was recently reported that autogenous bone grafts showed continuous volume reduction during the healing and follow-up periods. During maxillary sinus augmentation, the volume of autogenous grafts was reduced to 49.5% of the initial volume after 6 months (Johansson et al. 2001). In addition, it was demonstrated that the surgically augmented height with an autogenous block graft decreased to 60% after 10 months (Widmark et al. 1997).

The particle size of graft material has been regarded as one of the major factors that determine the ability of augmentation, and it has been studied by many researchers. However, these studies have reported variable conclusions so far. The aim of this study was to investigate the augmentation process and the ability of autogenous bone graft particles of two different sizes.

In the present study, TBV of the SB group decreased in a time-dependent manner; it decreased to 51.3% of the initial volume. Histological analysis showed that the grafted bone in the lower half had resorbed by multinuclear giant cells at 2 weeks, and was partially replaced by newly formed bone at 4 weeks. A great deal of newly formed bone had resorbed at 8 weeks. Thus, SB groups were considered to follow the remodeling process. In the upper part of the chamber, strongly stained SB observed at 2 weeks had resorbed by 4 weeks. This resorption caused volume reduction between 2 and 4 weeks. On the other hand, TBV of the LB group exhibited a volume increase at 4 weeks, and it was almost maintained at 8 weeks. Histologically, LB almost preserved its shape at 2 weeks and new bone formation was observed from the host bone to the LB surface at 4 weeks. The formation and resorption of bone was observed at 8 weeks. In addition, in the 4-week LB group, the original grafted bone of the upper half had the same low stainability, although numerous osteoclast-like cells were observed on the surface of the grafted bone. A greater part of the original grafted bone was maintained in the LB-grafted site at 8 weeks; meanwhile, the original grafted bone almost disappeared in the SB groups. This behavior of bone remodeling was thought to cause the difference in TBV between LB and SB.

The larger particle size of the grafting material was more beneficial than the small size bone grafts in augmentation. Demineralized freeze-dried bone allografts

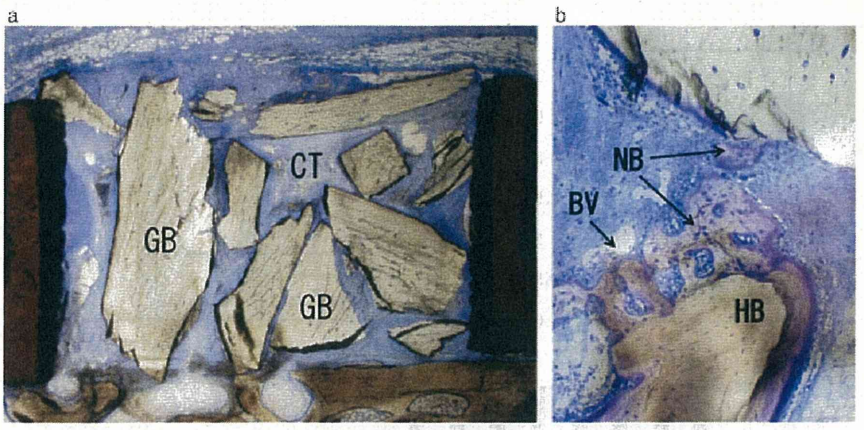

Fig. 6. Large bone grafted site at 2 weeks. (a) Grafted bone (GB) almost preserved its original shape. In the interspace of the GB, fibrous connective tissue (CT) was observed. Magnification × 2.5. (b) High-magnification image of (a). In the region close to the host bone (HB), blood vessels (BV) were found, and new bone (NB) formation occurred from the host bone surface to the GB surface. Magnification × 25.

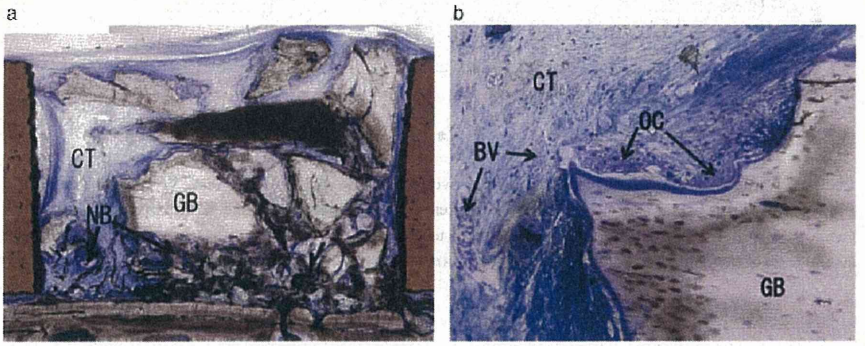

Fig. 7. Large bone grafted site at 4 weeks. (a) The center of grafted bone (GB) retained its original form. Fibrous connective tissue (CT) was observed around GB. A large amount of new bone (NB) was formed from the host bone surface to the GB surface. Magnification × 2.5. (b) High-magnification image of (a). Howship's lacunae with osteoclast-like cells (OC) were found at the surface of GB. Fibrous connective tissue and blood vessels (BV) were observed around the GB. Magnification × 40.

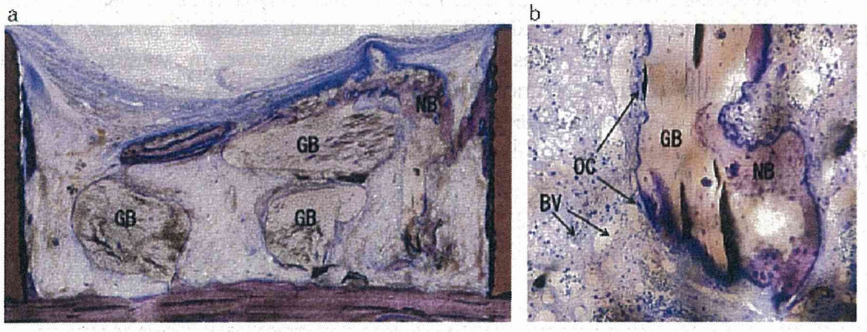

Fig. 8. Large bone grafted site at 8 weeks. (a) Newly formed bone (NB) was observed around the grafted bone (GB). GB was covered by NB, and many osteocytes were observed. Magnification × 2.5. (b) High-magnification image of (a). Osteoclast-like cells (OC) were observed on the surface of the GB. Around this bone architecture, many blood vessels (BV) were observed. Magnification × 40.

with 850–1000 μm particles yielded favorable results than the 250–500 μm particles in human periodontal defects (Fucini et al. 1993). Unmilled bone particle had more osteoblast than milled and drilled bone (Springer et al. 2004). In another study, application of 250–500 μm particle β-tricalcium phosphate particles exhibited more advantages in terms of bone formation than the 100–250 μm-sized particles (Murai et al. 2006). These results agree with the present study. However, the observations about particle size varied. In a rabbit autogenous graft defect model, there was no difference between the non-graft control, collected debris and particles collected by a manual bone crusher (Coradazzi et al. 2007). In addition, no significant difference was detected between the control defect and two sizes of β-tricalcium phosphate particles, 500–1000 and 1000–2000 μm, applied to a cynomolgus monkey mandible defect model (Kuroki et al. 2008). In these two studies, augmentation material was applied to the defect model, which was different from the chamber model in other studies, and is considered not suitable for confirming the augmentation potency. Hence, it would appear that application of large graft materials is preferable for bone augmentation. However, Pallesen et al. (2002) reported that 0.5–2.0 mm^3 particle autogenous bone exhibited more newly formed bone than 10 mm^3 in a rabbit cranial defect model. Thus, excessively large particles applied to a bone defect might have lower augmentation ability.

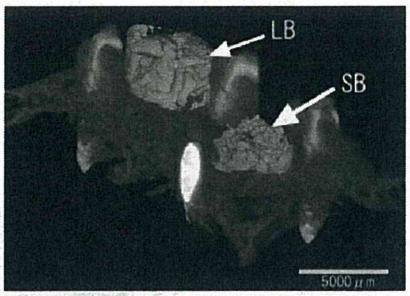

Fig. 9. Extracted image of bone-grafted site with micro-computed tomography (micro-CT). Both small bone (SB)- and large bone (LB)-grafted sites were extracted with micro-CT (grafted site image at 4 weeks).

The SB groups showed a considerable reduction of bone volume in the upper half of the chamber. The bone volumes of the upper half were 50.2%, 45.1%, 25.8% and 18.1% at 1, 2, 4 and 8 weeks, respectively. For this reason, BH of SB decreased at all experimental time points. Advanced biodegradability of small-sized grafted bone is considered to be responsible for these results. In contrast, LB could maintain the original shape of grafted bone in the upper half of the chamber; thus, BH was preserved during the entire period. Although the biodegradability of a bone substitute is

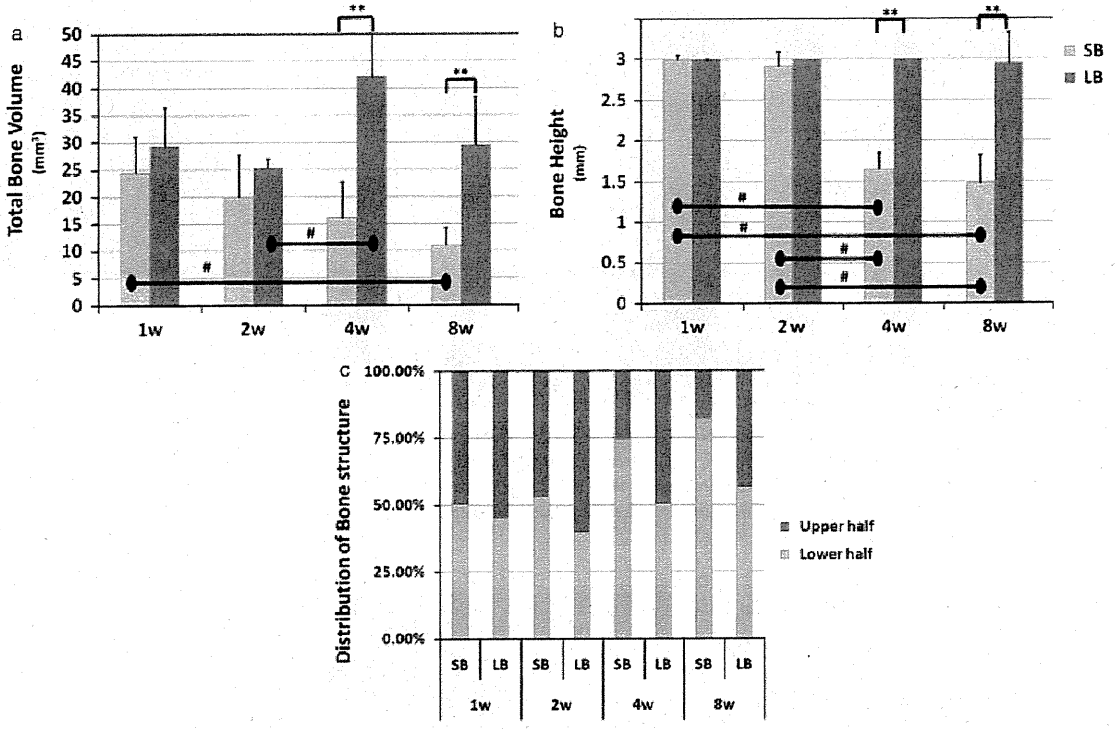

Fig. 10. Micro-computed tomography analysis. (a) Total bone volume change. Comparison between two groups – Mann–Whitney test, $^{**}P<0.01$; comparison within each group – non-parametric multiple comparison test, $^{\#}P<0.05$. Error bar indicates 95% confidence interval. (b) Bone height change. Comparison between two groups – Mann–Whitney test, $^{**}P<0.01$; comparison within each group – non-parametric multiple comparison test, $^{\#}P<0.05$. Error bar indicates 95% confidence interval. (c) Distribution of bone structure. Notably, bone volume reduction of the upper half was observed in small bone (SB) models. In contrast, large bone (LB) models exhibited no dramatic change.

thought to be very important, taking into account the volumetric augmentation ability, morphological stability is essentially required.

Clinically, autogenous bone is believed to be the gold standard for bone augmentation. However, the augmentation ability could differ with particle size. The present study indicates that small autogenous bone debris would be easily resorbed, having a poor outcome for augmentation. Therefore, to achieve sufficient bone augmentation, small autogenous bone debris should be applied in combination with a slow or a non-resorbable bone substitute. On the other hand, LB exhibited favorable augmentation with morphological stability. However, the osteogenesis in the interspace of grafted LB was limited, and newly trabecula formation progressed slowly throughout the entire experimental period. Therefore, to enhance osteogenesis in the interspace, application of SB might be effective.

Within the limitations of the present study, it is concluded that SB decreased to 51.3% and 51.0% of the initial volume and height, respectively, and LB could maintain the volume and height at 8 weeks in this augmentation model. SB follows smooth osteogenic process, whereas it is not effective in volume augmentation. However, LB is superior to SB in augmentation ability, although further studies are needed to evaluate the longitudinal bone augmentation condition.

References

Boronat-Lopez, A., Carrillo, C., Peñarrocha, M. & Peñarrocha-Diago, M. (2009) Immediately restored dental implants for partial-arch applications: a study of 12 cases. *Journal of Oral and Maxillofacial Surgery* **67**: 195–199.

Boyne, P. & James, R. (1980) Grafting of the maxillary sinus floor with autogenous marrow and bone. *Journal of Oral Surgery* **38**: 613–616.

Chiapasco, M., Consolo, U., Bianchi, A. & Ronchi, P. (2004) Alveolar distraction osteogenesis for the correction of vertically deficient edentulous ridges: a multicenter prospective study on humans. *International Journal of Oral & Maxillofacial Implants* **19**: 399–407.

Coradazzi, L., Garcia, I.J. & Manfrin, T. (2007) Evaluation of autogenous bone grafts, particulate or collected during osteotomy with implant burs: histologic and histomorphometric analysis in rabbits. *International Journal of Oral & Maxillofacial Implants* **22**: 201–207.

Ferrigno, N., Laureti, M., Fanali, S. & Grippaudo, G. (2002) A long-term follow-up study of non-submerged ITI implants in the treatment of totally edentulous jaws. Part I: ten-year life table analysis of a prospective multicenter study with 1286 implants. *Clinical Oral Implants Research* **13**: 260–273.

Fucini, S., Quintero, G., Gher, M., Black, B. & Richardson, A. (1993) Small versus large particles of demineralized freeze-dried bone allografts in human intrabony periodontal defects. *Journal of Periodontology* **64**: 844–847.

Fugazzotto, P. & Vlassis, J. (2007) Report of 1633 implants in 814 augmented sinus areas in function for up to 180 months. *Implant Dentistry* **16**: 369–378.

Hämmerle, C., Jung, R., Yaman, D. & Lang, N. (2008) Ridge augmentation by applying bioresorbable

membranes and deproteinized bovine bone mineral: a report of twelve consecutive cases. *Clinical Oral Implants Research* **19**: 19–25.

Jemt, T. & Lekholm, U. (2003) Measurements of buccal tissue volumes at single-implant restorations after local bone grafting in maxillas: a 3-year clinical prospective study case series. *Clinical Implant Dentistry & Related Research* **5**: 63–70.

Johansson, B., Grepe, A., Wannfors, K. & Hirsch, J. (2001) A clinical study of changes in the volume of bone grafts in the atrophic maxilla. *Dentomaxillofacial Radiology* **30**: 157–161.

Kihara, H., Shiota, M., Yamashita, Y. & Kasugai, S. (2006) Biodegradation process of alpha-TCP particles and new bone formation in a rabbit cranial defect model. *Journal of Biomedical Material Research B Applied Biomaterial* **79**: 284–291.

Kuroki, H., Toda, I. & Suwa, F. (2008) Experimental study of bone defect repair process with different sizes of β-TCP granules. *Journals of Japanese Society of Oral Implantology* **21**: 21–31.

Lustmann, J. & Lewinstein, I. (1995) Interpositional bone grafting technique to widen narrow maxillary ridge. *International Journal of Oral & Maxillofacial Implants* **10**: 568–577.

Moy, P., Lundgren, S. & Holmes, R. (1993) Maxillary sinus augmentation: histomorphometric analysis of graft materials for maxillary sinus floor augmentation. *Journal of Oral and Maxillofacial Surgery* **51**: 857–862.

Murai, M., Sato, S., Fukase, Y., Yamada, Y., Komiyama, K. & Ito, K. (2006) Effects of different sizes of beta-tricalcium phosphate particles on bone augmentation within a titanium cap in rabbit calvarium. *Dentistry Material Journal* **25**: 87–96.

Pallesen, L., Schou, S., Aaboe, M., Hjørting-Hansen, E., Nattestad, A. & Melsen, F. (2002) Influence of particle size of autogenous bone grafts on the early stages of bone regeneration: a histologic and stereologic study in rabbit calvarium. *International Journal of Oral & Maxillofacial Implants* **17**: 498–506.

Rodriguez, A., Anastassov, G., Lee, H., Buchbinder, D. & Wettan, H. (2003) Maxillary sinus augmentation with deproteinated bovine bone and platelet rich plasma with simultaneous insertion of endosseous implants. *Journal of Oral and Maxillofacial Surgery* **61**: 157–163.

Scabbia, A. & Trombelli, L. (2004) A comparative study on the use of a HA/collagen/chondroitin sulphate biomaterial (Biostite) and a bovine-derived HA xenograft (Bio-oss) in the treatment of deep intra-osseous defects. *Journal of Clinical Periodontology* **31**: 348–355.

Springer, ING., Terheyden, H., Geiß, S., Härle, F., Hedderich, J. & Açil, Y. (2004) Particulated bone grafts – effectiveness of bone cell supply. *Clinical Oral Implants Research* **15**: 205–212.

Turunen, T., Peltola, J., Yli-Urpo, A. & Happonen, R. (2004) Bioactive glass granules as a bone adjunctive material in maxillary sinus floor augmentation. *Clinical Oral Implants Research* **15**: 135–141.

Walsh, W., Vizesi, F., Michael, D., Auld, J., Langdown, A., Oliver, R., Yu, Y., Irie, H. & Bruce, W. (2008) Beta-TCP bone graft substitutes in a bilateral rabbit tibial defect model. *Biomaterials* **29**: 266–271.

Widmark, G., Andersson, B. & Ivanoff, C. (1997) Mandibular bone graft in the anterior maxilla for single-tooth implants. Presentation of surgical method. *International Journal of Oral and Maxillofacial Surgery* **26**: 106–109.

Yildirim, M., Spiekermann, H., Biesterfeld, S. & Edelhoff, D. (2000) Maxillary sinus augmentation using xenogenic bone substitute material Bio-oss in combination with venous blood. A histologic and histomorphometric study in humans. *Clinical Oral Implants Research* **11**: 217–229.

Zaner, D. & Yukna, R. (1984) Particle size of periodontal bone grafting materials. *Journal of Periodontology* **55**: 406–409.

Myat Nyan
Daisuke Sato
Hidemichi Kihara
Tetsu Machida
Keiichi Ohya
Shohei Kasugai

Effects of the combination with α-tricalcium phosphate and simvastatin on bone regeneration

Authors' affiliations:
Myat Nyan, Daisuke Sato, Hidemichi Kihara, Tetsu Machida, Shohei Kasugai, Oral Implantology and Regenerative Dental Medicine, Tokyo Medical and Dental University, Tokyo, Japan
Myat Nyan, Shohei Kasugai, Center of Excellence Program for Frontier Research on Molecular Destruction and Reconstruction of Tooth and Bone, Tokyo Medical and Dental University, Tokyo, Japan
Keiichi Ohya, Section of Pharmacology, Department of Hard Tissue Engineering, Tokyo Medical and Dental University, Tokyo, Japan

Correspondence to:
Dr Myat Nyan
Oral Implantology and Regenerative Dental Medicine
Tokyo Medical and Dental University
1-5-45 Yushima, Bunkyo-ku
Tokyo 113-8549
Japan
Tel.: +81 3 5803 4664
Fax: +81 3 5803 4664
e-mail: myatnyan@gmail.com

Date:
Accepted 21 July 2008

To cite this article:
Nyan M, Sato D, Kihara H, Machida T, Ohya K, Kasugai S. Effects of the combination with α-tricalcium phosphate and simvastatin on bone regeneration. *Clin. Oral Impl. Res.* 20, 2009; 280–287.
doi: 10.1111/j.1600-0501.2008.01639.x

Key words: α-TCP, BMP-2, bone formation, bone regeneration, simvastatin

Abstract

Background: Although local application of statins stimulates bone formation, high dose of simvastatin induces inflammation.

Objective: A study was conducted to test the hypothesis that maximum bone regeneration with less inflammation would be achieved by combining an optimal dose of simvastatin with α-tricalcium phosphate (α-TCP), which is an osteoconductive biomaterial capable of releasing the drug gradually.

Material and methods: Bilateral 5-mm-diameter calvarial defects were created in adult Wistar rats and filled with preparations of different doses of simvastatin (0, 0.01, 0.1, 0.25 and 0.5 mg) combined with α-TCP particles or left empty. The animals were sacrificed at 2, 4 and 8 weeks and analyzed radiologically and histologically. Half of the animals of 4 and 8 weeks were labeled with fluorescence dyes and histomorphometrically analyzed.

Results: Simvastatin doses of 0.25 and 0.5 mg caused inflammation of the soft tissue at the graft site whereas control and other doses did not. The micro-CT analysis revealed that the α-TCP with 0.1 mg simvastatin (TCP-0.1) group yielded significantly higher bone volumes than untreated control group at all three time points (249%, 227% and 266% at 2, 4 and 8 weeks, respectively). The percentage of defect closure, bone mineral content and bone mineral density were also higher in the TCP-0.1 group than in the other groups.

Conclusion: When combined with α-TCP particles, 0.1 mg simvastatin is the optimal dose for stimulation of the maximum bone regeneration in rat calvarial defects without inducing inflammation and it could be applied as an effective bone graft material.

With the expanding application of dental implant treatment to rehabilitate edentulous and partially edentulous patients, the demand for effective biomaterials for bone augmentation is increasing because there are disadvantages in autogenous bone grafting, such as donor site morbidity and limited availability of harvestable bone. In order to develop a bone graft with enhanced osteogenic properties, alloplastic bone substitutes have been combined with molecules, which enhance and/or induce new bone formation. Among these molecules, BMP-2 has especially shown its beneficial effects on bone regeneration. However, there are still some problems to be solved: such as short shelf life, inefficient delivery to target cells and high price (Einhorn 2003).

If pharmacological compounds can upregulate the intrinsic growth factors to stimulate bone growth, the strategy to combine such compounds with an osteoconductive bone substitute would be more cost-effective for bone regeneration. Topically applied simvastatin, a cholesterol-lowering drug, has been shown to

stimulate BMP-2 and VEGF mRNA expression in osteoblasts and promote bone growth over mouse calvaria (Mundy et al. 1999; Sugiyama et al. 2000; Garrett et al. 2001; Ohnaka et al. 2001; Thylin et al. 2002; Maeda et al. 2003; Ghosh-Choudhury et al. 2007). Other studies have reported that local application of statins induced bone growth in intact mandible, promoted bone regeneration in bone defects and tooth extraction sockets, and hastened fracture repair (Wong & Rabie 2003; Sato et al. 2005; Stein et al. 2005; Wong & Rabie 2005a, 2005b; Bradley et al. 2007; Garrett et al. 2007; Ozec et al. 2007; Sugiyama et al. 2007).

In our previous study, 1 mg simvastatin combined with calcium sulfate caused substantial bone regeneration in rat calvarial defects; however, considerable extent of soft-tissue inflammation was also observed at the site of application (Nyan et al. 2007). Other studies also reported that high doses of local simvastatin induced not only bone growth but also inflammation (Thylin et al. 2002; Stein et al. 2005). We hypothesized that the beneficial effects of simvastatin on bone regeneration with less inflammation could be achieved by combining an optimal dose of simvastatin with a bone substitute, which can gradually release the drug into the local bone environment. To test this hypothesis, we chose α-tricalcium phosphate (α-TCP) to combine with simvastatin. Calcium phosphate materials, such as hydroxyapatite and TCP, have been widely used as bone substitutes in orthopedic and maxillofacial surgery, as these materials show high biocompatibility and osteoconductivity. α-TCP has been shown to be a gradually degradable osteoconductive material (Wiltfang et al. 2002; Kihara et al. 2006). The purpose of this study was to evaluate bone regeneration by different doses of simvastatin in combination with α-TCP particles in rat calvarial defects and to determine the optimal dose of simvastatin for maximum bone regeneration with less inflammation.

Material and methods

Preparation of α-TCP and simvastatin combination

α-TCP particles with a diameter of 500–700 μm were obtained from Advance Co., Tokyo, Japan. Simvastatin (OHARA Pharmaceutical Co. Ltd, Koka, Shiga, Japan) was dissolved in ethanol and the solution was applied to the α-TCP particles by dropping under sterile conditions. As the α-TCP particles have numerous fine pores, the solution was uniformly and quickly distributed into the material. α-TCP particles containing the following doses of simvastatin were prepared: 0.01, 0.1, 0.25 and 0.5 mg per 14 mg α-TCP particles.

Anesthesia and surgical procedures

This study was approved by the institutional committee for animal experiments. Sixty-nine Wistar adult rats (16 weeks old) were used. The animals were anesthetized with a combination of ketamine–xylazine (40 and 5 mg/kg). The dorsal part of the cranium was shaved and prepared aseptically for surgery. A 20-mm-long incision in the scalp along the sagittal suture was made, and the skin, subcutaneous tissue and periosteum were reflected, exposing the parietal bones. Two full-thickness bone defects of 5 mm diameter were trephined in the dorsal part of the parietal bone lateral to the sagittal suture. A 5 mm trephine bur was used to create the defects under constant irrigation with sterile physiologic solution to prevent overheating of the bone edges. Care was taken during the surgical procedure to prevent damage to dura mater. In nine animals, both defects were left untreated to serve as negative control (Fig. 1a). In 45 animals, both defects were filled with 14 mg of α-TCP or α-TCP combined with 0.01, 0.1, 0.25 or 0.5 mg simvastatin (Fig. 1b), designated as TCP-0, TCP-0.01, TCP-0.1, TCP-0.25 or TCP-0.5 group, respectively ($n = 9$ for each group). In 15 animals, one defect was used to test each of the above materials whereas the other defect was left untreated to observe whether simvastatin from filled defect influenced the healing of contralateral unfilled defect (Fig. 1c). The periosteum and subcutaneous tissues were sutured in place using 4-0 Vicryl polyglactin suture (Ethicon Inc., NJ, USA) and the scalp with 4-0 silk (ELP Akiyma Co., Tokyo, Japan).

Animals were observed daily for any appearance of clinical signs of inflammation, photographed and recorded. For bone histomorphometrical analysis, 7 days and 1 day before sacrifice, calcein and tetracycline were injected, respectively, in half of the animals with particle-filled defects in 4-week and 8-week groups.

Tissue harvest and radiological analyses

Animals were sacrificed at 2, 4 and 8 weeks after the surgery. The skin was dissected and the defect sites were removed along with surrounding bone and soft tissues. Then, X-ray imaging was performed by a micro-CT scanner (InspeXio; Shimadzu Science East Corporation, Tokyo, Japan) with a voxel size of 70 μm/pixel. Tri/3D-Bon software (RATOC System Engineering Co. Ltd, Tokyo, Japan) was used to make a 3D reconstruction from the obtained set of scans. Out of the entire 3D data set, a cylindrical region of interest (ROI) with a diameter of 5 mm and a height that covered the entire thickness of the calvarial bone was selected for analysis. ROI was placed where the original defect was located as the margins were visually recognizable. Mask work was performed to binarize the α-TCP particles and new bone in the ROI separately according to different intensity values, as the former was more dense and radio-opaque than the latter. Then, the region of new bone was extracted from the whole binarized ROI by the logic operation work and the volume was measured. Percentage of defect closure was also calculated according to micro-CT images. After micro-CT analysis, bone mineral content (BMC) and bone mineral density (BMD) in the defect region of the 8-week samples were measured by dual-energy

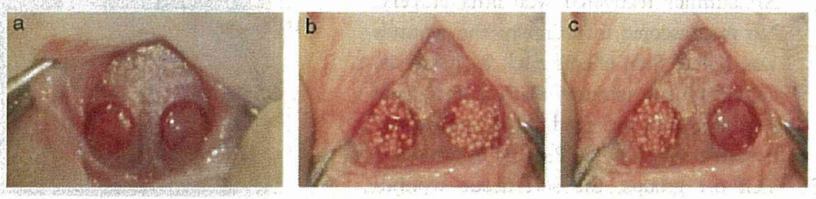

Fig. 1. Bilateral 5 mm diameter rat calvarial defect model. (a) Empty control defects, (b) particle-filled defects filled with 14 mg of α-tricalcium phosphate particles, (c) unfilled defect contralateral to particle-filled defect to assess the influence of particle-filled defect.

X-ray absorptiometry for small animals (DXA-DCS-600; Aloka Co. Ltd, Tokyo, Japan).

Histological evaluation

After the radiological analyses, the specimens were fixed in 10% neutralized formalin for 1 week. The specimens from the animals that had not received vital labeling were decalcified in 5% formic acid for 2 weeks and then embedded in paraffin. Before the embedding procedure, an incision was made exactly through the middle of the bone defects to ensure that the microtome sections were made in the area of interest. Coronal sections of about 5 μm thickness were prepared, stained with hematoxylin–eosin and observed under an optical microscope.

Measurement of mineral apposition rate (MAR)

After harvesting and fixation procedures, the specimens were dehydrated in graded alcohol and embedded in the GMA/MMA resin. Five-micrometer-thick sections were cut coronally and unstained sections were observed under a fluorescent microscope for fluorochrome labeling. For MAR, interlabel distance was measured and the value was divided by the time interval between administrations of two vital markers. Then, the sections were stained with 0.1% toluidine blue for microscopic observation.

Statistical analysis

Data were first analyzed by one-way ANOVA. When this analysis suggested a significant difference between groups ($P<0.05$), the data were further analyzed by the Tukey *post hoc* multiple comparison tests.

Results

Macroscopic observation

All animals recovered well after surgery. No macroscopic infection of the wounds was noted. Side effects such as paralysis, convulsions, respiratory distress or signs of pain were not observed. In all animals of negative control, TCP-0, TCP-0.01 and TCP-0.1 groups, the soft tissue wounds healed uneventfully without showing clinical signs of inflammation. Animals in TCP-0.5 and TCP-0.25 groups revealed redness of the skin overlying the bone defects at 3 and 5 days, respectively. Localized area of swelling became evident over those areas from the following day in both groups. The inflamed areas proceeded to form ulceration and scabbing. The ulcers and scabs became reduced in intensity until 10 days. Generally, inflammation and scab formation were less intense in TCP-0.25 group and the soft tissue wounds healed 2–3 days earlier than those of TCP-0.5 group. At 2 weeks, the wounds showed complete soft tissue healing with the disappearance of swelling and/or scabbing.

Radiological observation

Control group

Scanty amount of new bone was formed in some areas along the margin of bone defect at 2 and 4 weeks (Fig. 2Ia and IIa). At 8 weeks, more new bone formation was observed with the thin layer of bone extending towards the center. However, there was no complete defect closure (Fig. 2IIIa).

TCP-0 and TCP-0.01 groups

Newly formed bone and grafted α-TCP particles could be easily differentiated as they revealed different radiopacity. At 2 and 4 weeks, only a small area of new bone was seen at the defect margins in both groups (Figs 2Ib and c and IIb and c). The bone formation became more evident at 8 weeks at the defect margins and around the TCP particles most of which appeared to be reduced in size but still present in the defect (Fig. 2IIIb and c).

TCP-0.1 group

At 2 weeks, the new bone was formed not only at the margin of the defect but also in between the α-TCP particles close to the

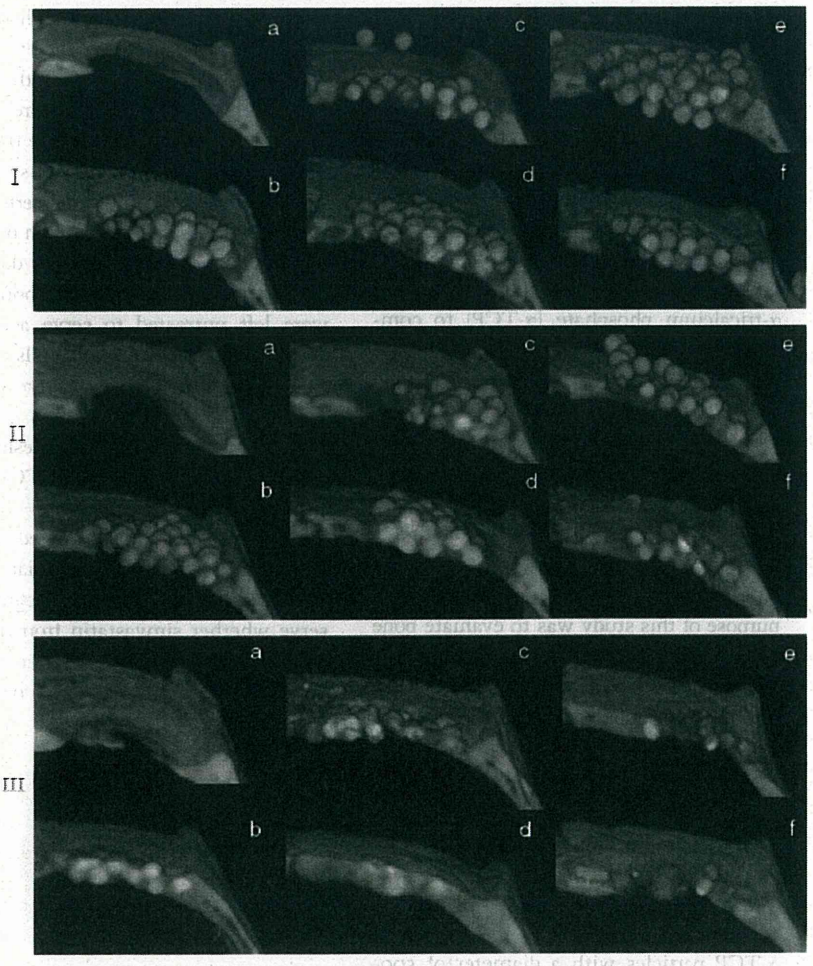

Fig. 2. Micro-CT images of bone defects at (I) 2 weeks, (II) 4 weeks and (III) 8 weeks. (a) Control, (b) TCP-0, (c) TCP-0.01, (d) TCP-0.1, (e) TCP-0.25, (f) TCP-0.5 groups. The images were trimmed to show the center of each defect. TCP, tricalcium phosphate.

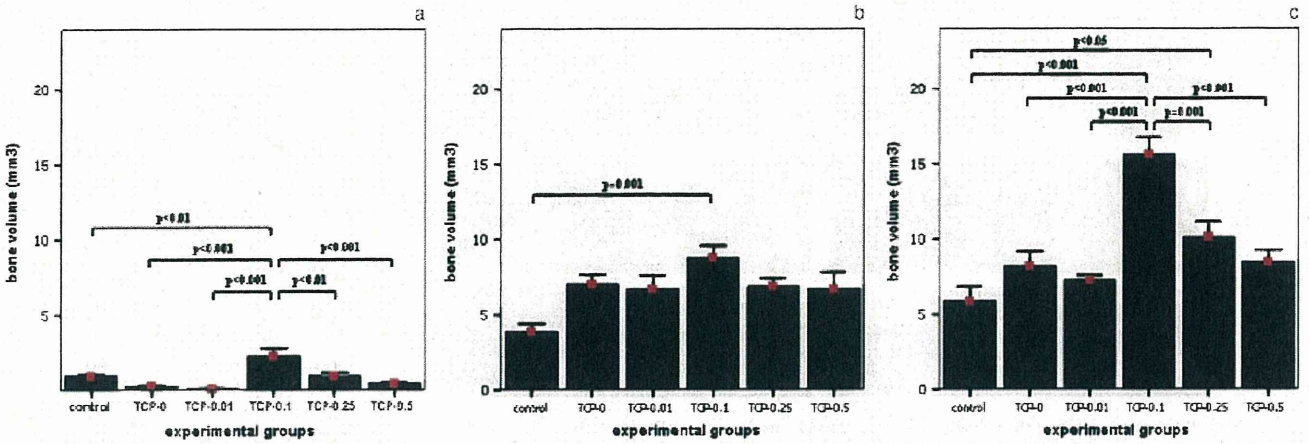

Fig. 3. Bone volume in the defect at (a) 2 weeks (b) 4 weeks and (c) 8 weeks. Bone volume was measured in micro-CT images three-dimensionally. Bars and error bars represent means and SEM, respectively. $n = 7$ in each particle-filled group and $n = 6$ in the control group at each time point. ANOVA 2 weeks ($F_{5,35} = 10.655$, $P < 0.0001$), 4 weeks ($F_{5,35} = 3.861$, $P = 0.007$), 8 weeks ($F_{5,35} = 14.437$, $P < 0.0001$).

dura mater (Fig. 2.Id). New bone continued to form between the defect margin and the α-TCP particles at 4 weeks. Bone had also penetrated in between the particles at the center of defect and resulted in almost a complete 3D closure of the defect (Fig. 2IId). At 8 weeks, most defects from TCP-0.1 group achieved complete defect closure by continued formation of new bone around the remaining α-TCP particles as well as in place of resorbed α-TCP particles at the center of defect. There were only a few remaining α-TCP particles demonstrating more diffused borders and reduced in size (Fig. 2IIId).

TCP-0.25 and TCP-0.5 groups

At 2 weeks, only a scanty amount of new bone was observed at the defect margins (Fig. 2Ie and f). More bone formation became evident at 4 and 8 weeks at the margins without achieving complete defect closure (Figs 2IIe and f and 3IIIe and f).

Radiographic bone volume, defect closure, BMC and BMD

Figure 3 shows the mean bone volumes measured in the micro-CT images at 2, 4 and 8 weeks. The TCP-0.1 group yielded significantly higher bone volumes than untreated control group at all time points (249%, 227% and 266% at 2, 4 and 8 weeks, respectively). At 2 and 8 weeks, the TCP-0.1 group showed significantly higher bone volume than all other groups.

Table 1 demonstrates the percentage of defect closure, BMC and BMD, which were all evaluated at 8 weeks. The percentage of defect closure was significantly higher in TCP-0.1 group than control and TCP-0.5 groups. Moreover, the BMC and BMD values were also significantly higher in TCP-0.1 group than control, TCP-0 and TCP-0.01 groups. TCP-0.25 group also showed higher percentage of defect closure and BMC than control group.

***Table 1*. Percentage of defect closure, bone mineral content (BMC) and bone mineral density (BMD) of the defect at 8 weeks ($n = 7$ for each particle-filled group and $n = 6$ for control group)**

Experimental groups	Defect closure (%)	BMC (mg)	BMD (mg/cm^2)
Control	41.67 ± 10.78	21.35 ± 0.89	66.05 ± 1.99
TCP-0	74.29 ± 9.48	24.74 ± 1.15	74.97 ± 3.51
TCP-0.01	74.29 ± 6.4	24.71 ± 1.05	74.94 ± 3.17
TCP-0.1	97.86 ± 1.49	29.07 ± 1.11	88.07 ± 3.35
TCP-0.25	82.14 ± 5.55	25.74 ± 1.05	78.01 ± 3.16
TCP-0.5	63.57 ± 9.3	25.49 ± 0.61	77.26 ± 1.84

†$P < 0.01$,
*$P < 0.05$.
Values are shown as mean ± SEM.
ANOVA percentage of defect closure ($F_{5,35} = 5.724$, $P = 0.001$), BMC ($F_{5,35} = 5.82$, $P = 0.001$), BMD ($F_{5,35} = 5.483$, $P = 0.001$).

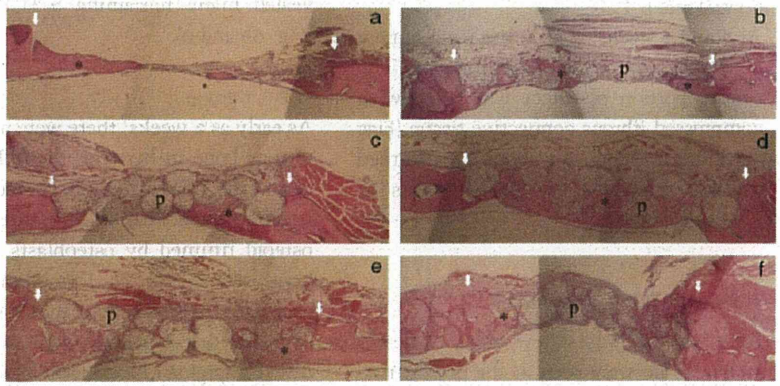

Fig. 4. Photomicrographs of the calvarial defects at 2 weeks representing (a) control, (b) TCP-0, (c) TCP-0.01, (d) TCP-0.1, (e) TCP-0.25 and (f) TCP-0.5 groups. Arrows denote original defect margins. *Newly formed bone; P the α-TCP particle. (Hematoxylin and eosin stain, original magnification × 4).TCP, tricalcium phosphate.

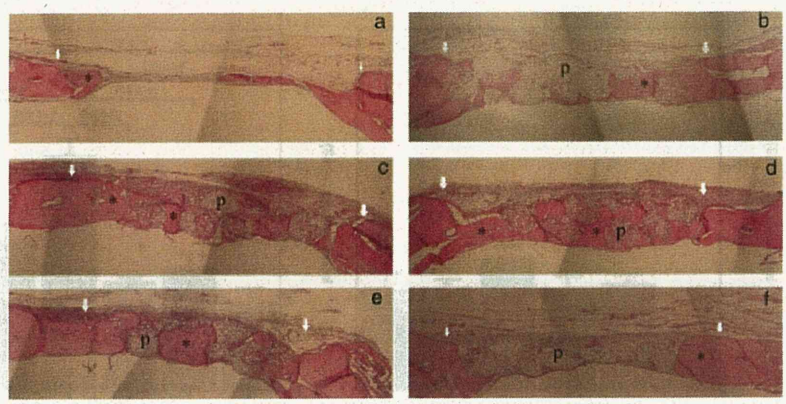

Fig. 5. Photomicrographs of the calvarial defects at 4 weeks representing (a) control, (b) TCP-0, (c) TCP-0.01, (d) TCP-0.1, (e) TCP-0.25 and (f) TCP-0.5 groups. Arrows denote original defect margins. *Newly formed bone; P the α-TCP particle. (Hematoxylin and eosin stain, original magnification × 4).

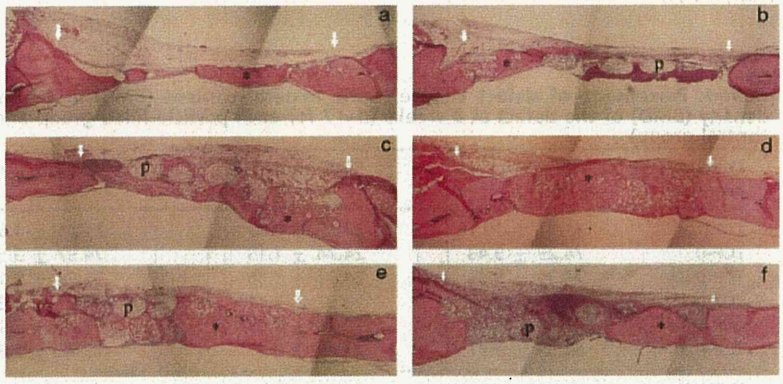

Fig. 6. Photomicrographs of the calvarial defects at 8 weeks representing (a) control, (b) TCP-0, (c) TCP-0.01, (d) TCP-0.1, (e) TCP-0.25 and (f) TCP-0.5 groups. Arrows denote original defect margins. *Newly formed bone; P the α-TCP particle. (Hematoxylin and eosin stain, original magnification × 4). TCP, tricalcium phosphate.

Histological observation

Control group

At 2 and 4 weeks, only a thin layer of new bone was seen at the defect margins. The central portion of defect was filled with compressed fibrous connective tissue (Figs 4a and 5a). More new bone was formed towards the center in some defects at 8 weeks (Fig. 6a).

TCP-0 and TCP-0.01 groups

At 2 weeks, only a few areas of newly formed bone were seen at the defect margins and between some adjacent α-TCP particles in TCP-0 group. Each particle demonstrated many spaces inside it forming a reticulate structure. Only a few inflammatory cells were noted generally in the soft tissue (Fig. 4b and c). The areas of new bone became increased at 4 weeks (Fig. 5b and c). Although new bone formation appeared to continue from the defect margins at 8 weeks, both groups still revealed many remaining α-TCP particles (Fig. 6b and c).

TCP-0.1 group

As early as 2 weeks, there were many areas of new bone in between the α-TCP particles in the TCP-0.1 group, characterized by irregular trabeculae of immature bone and osteoid rimmed by osteoblasts. The new bone seemed to be formed abundantly especially near the dura mater surface all over the defect area as well as from the defect margins. Numerous blood vessels were also associated with the newly formed bone. Active osteoblasts lined around the surface of the α-TCP particles and bone matrix appeared to be deposited inside some particles located near the bottom of the defect. At the defect borders, bone had bridged the gap between the defect border and the inserted α-TCP particles. Only a few inflammatory cells were observed in the soft tissue covering the defect (Fig. 4d). At 4 weeks, more advanced bone formation was seen at the center of defects. Moreover, bone matrix appeared to be deposited inside all α-TCP particles in the defect (Fig. 5d). At 8 weeks, most of the defects showed a complete bridging of new bone across the defect by continuous regeneration of bone at the center. New bone was also observed inside the remaining α-TCP particles. Thus, the latter appeared to be partially obliterated by bone (Fig. 6d).

TCP-0.25 and TCP-0.5 groups

At 2 weeks, only a few areas of new bone were seen at the defect margins. There were many inflammatory cells and fibroblasts in the soft tissue covering the defect and also in between some α-TCP particles, which were located close to the soft tissue. Some inflammatory cells infiltrated inside the α-TCP particles. Many collagen fibers filled the space in between the α-TCP particles. The inflammatory cell infiltration was more prominent and extensive in TCP-0.5 group (Fig. 4e and f). At 4 weeks, the inflammatory cells were markedly reduced and more new bone was formed at the margin as well as in some areas at the center of the defect in TCP-0.25 group (Fig. 5e). In TCP-0.5 group, however, the amount of new bone did not increase showing many α-TCP particles, which were still invaded by fibroblasts and some inflammatory cells (Fig. 5f). At 8 weeks, a considerable amount of bone was formed in the TCP-0.25 group, but there was no complete bridging of the defect with some remaining particles at the center (Fig. 6e). More bone was formed in TCP-0.5 group at this time point compared with that of 4 weeks; however, the areas of remaining α-TCP particles still predominated the defect (Fig. 6f).

MAR

MAR values were shown in Fig. 7. Consistent with the higher bone volume in TCP-0.1 group, the MAR in this group was significantly higher than those of all other groups at 4 weeks. At 8 weeks, however, there was no statistically significant difference between TCP-0.1 and TCP-0.25 groups whereas other groups (TCP-0, TCP-0.01 and TCP-0.5) still showed significantly lower MARs than that of TCP-

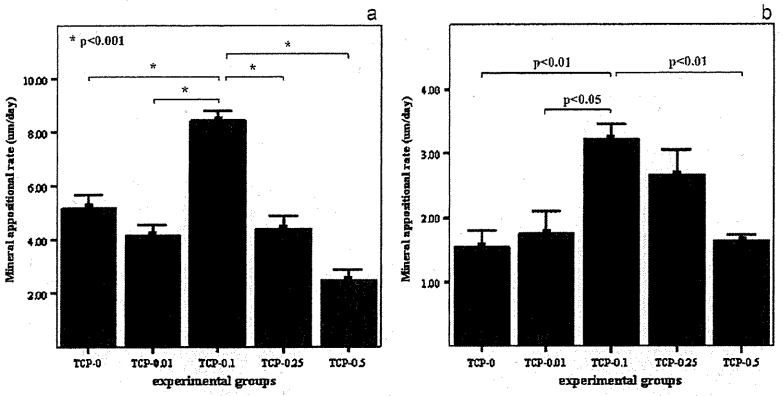

Fig. 7. Mineral apposition rates at (a) 4 weeks and (b) 8 weeks. Bars and error bars represent means and SEM, respectively. $n = 4$ for each group at each time point. ($F_{4,15} = 6.978$, $P = 0.002$).

0.1 group. Relatively higher apposition rate in the TCP-0.25 group at 8 weeks was in line with the increasing bone volume in this group at 8 weeks. In all groups, MARs decreased at 8 weeks compared with those at 4 weeks (Fig. 7a and b).

Discussion

Bone regeneration requires three essential components: firstly, signaling molecule; secondly, scaffold which acts as osteoconductive surface to support osteoblastic bone formation; and thirdly, cells responsible for bone formation. Our strategy is *in situ* tissue regeneration approach in which new tissue formation is induced by specific scaffolds with external stimuli that are used to stimulate body's own cells and promote local tissue repair. We applied different doses of simvastatin combined with osteoconductive α-TCP particles in rat calvarial defects and showed that 0.1 mg simvastatin induced maximum bone regeneration.

Simvastatin is one of the commonly prescribed cholesterol lowering drugs and it has been shown to upregulate BMP-2 and VEGF gene expression in osteoblasts (Mundy et al. 1999; Sugiyama et al. 2000; Garrett et al. 2001; Ohnaka et al. 2001; Maeda et al. 2001, 2003; Ghosh-Choudhury et al. 2007). Administration of statins either systemically or locally has been shown to promote bone growth and/or regeneration (Skoglund et al. 2002; Thylin et al. 2002; Wong & Rabie 2003; Knoch et al. 2005; Sato et al. 2005; Stein et al. 2005; Wong & Rabie 2005a, 2005b; Bradley et al. 2007; Garrett et al. 2007; Nyan et al. 2007; Ozec et al. 2007; Sugiyama et al. 2007). Simvastatin was chosen as the statin to be tested in our study because *in vitro* studies have shown it to be one of the most potent statins in stimulating bone growth (Garrett et al. 2001) and other *in vivo* studies have confirmed its bone-promotive effect.

Although anti-inflammatory effects of statins have been reported (Weitz-Schmidt 2002), high-dose simvastatin induces inflammation around the site of local application. It has been shown that local simvastatin application at 2.2 mg causes inflammation and scabbing of the skin overlying the murine calvaria (Thylin et al. 2002). Stein et al. (2005) applied simvastatin in methyl cellulose gel in a polylactic acid membrane locally on rat mandible at different doses and found that by lowering the simvastatin dose, the signs of inflammation can be reduced and they concluded that 0.5 mg simvastatin is the optimal dose for single local application. In our previous study, 1 mg simvastatin combined with calcium sulfate caused substantial bone regeneration in rat calvarial defects; however, with a considerable soft-tissue inflammation and scabbing of the skin overlying the calvaria (Nyan et al. 2007). Thus, the local effects of simvastatin would be dose- and carrier-dependent. We speculate that a carrier degrading rapidly during the early phase of bone healing would not be desirable for bone regeneration with simvastatin.

Calcium phosphate materials have been shown to be osteoconductive and highly biocompatible (LeGeros 2002) and these materials have been successfully applied as carriers for antibiotics and growth factors such as BMPs (Downes et al. 1991; Guicheux et al. 1998; Blom et al. 2000; Laffargue et al. 2000; Yan et al. 2004; Ginebra et al. 2006; Saito et al. 2006). Among the different calcium phosphate materials, we used α-TCP particles in this study because previous studies have confirmed the role of α-TCP particles as bone-rebuilding material by gradual biodegradation and formation of bone around them (Wiltfang et al. 2002; Kihara et al. 2006). α-TCP is also reported to be able to induce efficient growth of bone cells, and the production of an environment that stimulates osteogenesis *in vitro* (Mayr-Wohlfart et al. 2001; Ehara et al. 2003).

We used rat bilateral calvarial defect model to test our hypothesis, as it is a convenient model for the study of bone-regenerative materials because of its lack of fixation requirements. Experimental models with very young animals are considered unsatisfactory to evaluate osteopromotive materials. The animals used in this study were at adult stage (16 weeks); therefore, increased bone regeneration attributed to growth is not expected.

In our experiment, maximum bone regeneration was consistently observed in the defects applied with the combination of 0.1 mg simvastatin and α-TCP. It is likely to be a result of maximum stimulation of osteoblasts by locally released simvastatin to promote production of BMP-2 and VEGF. In the histological sections of the 2-week samples, many active osteoblasts were observed bordering around the surface of α-TCP particles and depositing bone matrix actively. Osteoblasts originate from osteoprogenitor cells in the bone marrow stroma termed BMSCs or mesenchymal stem cells, and *in vitro* studies have shown that simvastatin promotes osteoblastic differentiation in the human BMSCs and enhances the mineralization of the matrix by the osteoblasts (Song et al. 2003; Baek et al. 2005). We also observed significantly increased MARs in this group suggesting the increased activity of individual osteoblasts.

Stein et al. (2005) demonstrated that 0.1 mg simvastatin clearly showed only a minimal inflammation in terms of swelling and infiltrated area, but little bone growth than the control. The results of our study

are consistent with their observation except the finding that 0.1 mg simvastatin induced the significantly highest bone formation in our study. This difference may be due to the experimental model and simvastatin carrier. They applied simvastatin on the periosteum of intact mandible whereas we applied it in the bone defect. As simvastatin carrier, they used methyl cellulose gel whereas we used α-TCP particles that might be expected releasing the drug efficiently in the bone defect.

Studies on release of proteins from calcium phosphate materials reported a biphasic manner of release; an initial rapid release followed by a gradual long-lasting one (Downes et al. 1991; Guicheux et al. 1998; Blom et al. 2000; Laffargue et al. 2000; Ziegler et al. 2002). It is also likely that a burst initial dose of adsorbed simvastatin was released by α-TCP in early phase of healing in our experiment. Such a release of simvastatin may be advantageous in TCP-0.1 group for providing an optimal dose of the drug that could stimulate local responding cells to express BMP-2 without eliciting an inflammatory reaction. Bone regeneration was apparent in this group since the earliest observation period of 2 weeks. Furthermore, significantly higher values of bone volume at later time points in TCP-0.1 group suggested a maximum stimulation of the local cells by simvastatin. Possibly, sustained release of simvastatin from the gradually degrading α-TCP particles might have provided continued exposure of local osteoblasts to simvastatin resulting in the upregulation of BMP-2 and subsequent stimulation of migrated mesenchymal cells to osteoblastic differentiation. Interestingly, the regenerated bone at 8 weeks seemed to be self-limited by remodeling so that the normal contour of bone surface was achieved.

Notably, the degradation and disappearance of α-TCP particles was the most evident in TCP-0.1 in which bone formation was the most prominent. In this particular group, it is likely that bone remodeling together with bone formation was remarkably enhanced. As a result, α-TCP particles might be rapidly degraded and exchanged to new bone in this group.

In contrast, the released simvastatin from TCP-0.25 and TCP-0.5 groups seemed to cause exacerbation of the normal inflammatory reaction in local wound environment in the early phase of bone healing. Although inflammation is the initiator of healing, an excessive or aberrant inflammatory response is well recognized as a major contributing factor to delayed healing in both animal and human models (Szpaderska & DiPietro 2005; Eming et al. 2007; Menke et al. 2007). Bunn et al. (2005) reported that bone healing was impaired in the fracture model associated with overlying muscle crush injury in which the excess inflammation caused increased production of inflammatory cytokines. In our study, despite the promotion of BMP-2 expression by simvastatin, the excessive inflammation in the higher-dose groups might have induced the production of inflammatory cytokines, excess of which may be deleterious for differentiation and/or subsequent mineralization of osteoblasts. The net result was less new bone formation in these groups compared with TCP-0.1 group, not only in the early phase but also in the later time points. The difference was more obvious in defects grafted with 0.5 mg simvastatin with α-TCP in which more intense and prolonged inflammation had been observed. On the other hand, 0.01 mg simvastatin appeared to be insufficient to stimulate bone healing in this experiment.

In addition to the effects of locally released simvastatin, bioactivity and osteoconductivity of α-TCP particles may also play an important role in the maximum bone regeneration in TCP-0.1 group. It is well established that partial dissolution of calcium phosphate biomaterials causes liberation of calcium and phosphate ions into the microenvironment, which in term promotes bone mineralization and enhances bone formation (LeGeros 2002). As we had reported previously (Kihara et al. 2006), the new bone was formed on the surface of TCP particles and inside the particles in the present study, which further supports the osteoconductivity of α-TCP particles.

The outcome of any type of regenerative procedure is strongly dependent upon the available space under the mucoperiosteal flap (Wikesjo & Selvig 1999). In the present study, the flap collapse in particle-filled defects seemed to be prevented by the use of α-TCP particles as we had observed in the previous study (Kihara et al. 2006). All the particle-filled defects yielded more bone regeneration than empty control defects. This space-maintaining property of α-TCP is advantageous in the bone augmentation procedures.

The empty defects in the negative control group and the defect adjacent to the positive control (α-TCP only) group revealed formation of only a thin layer of new bone along the periphery of defect. Notably, the unfilled empty defects contralateral to those filled with simvastatin–TCP combination showed considerable bone regeneration and healed well (data not shown). This finding suggested a possible paracrine manner of bone formation-stimulating signal from the filled defects with simvastatin–TCP combination.

In conclusion, our study confirmed the bone promoting effect of local simvastatin and determined that 0.1 mg was the optimal dose for the maximum bone regeneration of 5-mm-diameter bone defects in rat calvaria when applied in combination with α-TCP. Further studies are required to validate the effect of this optimal dose of simvastatin with α-TCP combination in different clinical situations.

Acknowledgements: This research was supported by the grant for Center of Excellence Program for Frontier Research on Molecular Destruction and Reconstruction of Tooth and Bone in Tokyo Medical and Dental University and by a Grant (19390513) from the Ministry of Education, Science and Culture, Japan.

References

Baek, K.H., Lee, W.Y., Oh, K.W., Tae, H.J., Lee, J.M., Lee, E.J. & Han, J.H. (2005) The effect of simvastatin on the proliferation and differentiation of human bone marrow stromal cells. *Journal of Korean Medical Science* 20: 438–444.

Blom, E.J., Klein-Nulend, J., Klein, C.P., Kurashina, K., van Waas, M.A. & Burger, E.H. (2000) Transforming growth factor-beta1 incorporated during setting in calcium phosphate cement stimulates bone cell differentiation in vitro. *Journal of Biomedical Materials Research* **50**: 67–74.

Bradley, J.D., Cleverly, D.G., Burns, A.M., Helm, N.B., Schmid, M.J., Marx, D.B., Cullen, D.M. & Reinhardt, R.A. (2007) Cyclooxygenase-2 inhibitor reduces simvastatin-induced bone morphogenic protein-2 and bone formation *in vivo*. *Journal of Periodontal Research* **42**: 267–273.

Bunn, R.J., Burke, G., Connelly, C., Li, G. & Marsh, D. (2005) Inflammation-A double edged sword in high-energy fractures? *Journal of Bone and Joint Surgery – British Volume* **87-B** (Suppl. III): 265–266.

Downes, S., DiSilvio, L., Klein, C.P.A.T. & Kayser, M.V. (1991) Growth hormone loaded bioactive ceramics. *Journal of Materials Science: Materials in Medicine* **2**: 176–180.

Ehara, A., Ogata, K., Imazato, S., Ebisu, S., Nakano, T. & Umakoshi, Y. (2003) Effects of α-TCP and TetCP on MC3T3-E1 proliferation, differentiation and mineralization. *Biomaterials* **24**: 831–836.

Einhorn, T.A. (2003) Clinical applications of recombinant human BMPs: early experience and future development. *Journal of Bone Joint Surgery (Am)* **85** (Suppl. 3): 82–88.

Eming, S.A., Krieg, T. & Davidson, J.M. (2007) Inflammation in wound repair: molecular and cellular mechanisms. *Journal of Investigative Dermatology* **127**: 514–525.

Garrett, I.R., Gutierrez, G. & Mundy, G.R. (2001) Statins and bone formation. *Current Pharmacological Design* **7**: 715–736.

Garrett, I.R., Gutierrez, G.E., Rossini, G., Nyman, J., McCluskey, B., Flores, A. & Mundy, G.R. (2007) Locally delivered lovastatin nanoparticles enhance fracture healing in rats. *Journal of Orthopedic Research* **25**: 1351–1357.

Ghosh-Choudhury, N., Mandal, C.C. & Choudhury, G.G. (2007) Statin-induced Ras activation integrates the phosphatidylinositol 3-kinase signal to Akt and MAPK for bone morphogenetic protein-2 expression in osteoblast differentiation. *Journal of Biological Chemistry* **282**: 4983–4993.

Ginebra, M.P., Traykova, T. & Planell, J.A. (2006) Calcium phosphate cements as bone drug delivery systems: a review. *Journal of Controlled Release* **113**: 102–110.

Guicheux, J., Gauthier, O., Aguado, E., Heymann, D., Pilet, P., Couillaud, S., Faivre, A. & Daculsi, G. (1998) Growth hormone-loaded macroporous calcium phosphate ceramic: *in vitro* biopharmaceutical characterization and preliminary in vivo study. *Journal of Biomedical Materials Research* **40**: 560–566.

Kihara, H., Shiota, M., Yamashita, Y. & Kasugai, S. (2006) Biodegradation process of α-TCP particles and new bone formation in a rabbit cranial defect model. *Journal of Biomedical Materials Research Part B: Applied Biomaterials* **79B**: 284–291.

Knoch, von F., Wedemeyer, C., Heckelei, A., Saxler, G., Hilken, G. & Brankamp, J., et al. (2005) Promotion of bone formation by simvastatin in polyethylene particle-induced osteolysis. *Biomaterials* **26**: 5783–5789.

Laffargue, P., Fialdes, P., Frayssinet, P., Rtaimate, M., Hildebrand, H.F. & Marchandise, X. (2000) Adsorption and release of insulin-like growth factor-I on porous tricalcium phosphate implant. *Journal of Biomedical Materials Research* **49**: 415–421.

LeGeros, R.Z. (2002) Properties of osteoconductive biomaterials: calcium phosphates. *Clinical Orthopaedics and Related Research* **395**: 81–98.

Maeda, T., Kawane, T. & Horiuchi, N. (2003) Statins augment vascular endothelial growth factor expression in osteoblastic cells via inhibition of protein prenylation. *Endocrinology* **144**: 681–692.

Maeda, T., Matsunuma, A., Kawane, T. & Horiuchi, N. (2001) Simvastatin promotes osteoblast differentiation and mineralization in MC3T3-E1 Cells. *Biochemical and Biophysical Research Communications* **280**: 874–877.

Mayr-Wohlfart, U., Fiedler, J., Gunther, K.P., Puhl, W. & Kessler, S. (2001) Proliferation and differentiation rates of a human osteoblast-like cell line (SaOS-2) in contact with different bone substitute materials. *Journal of Biomedical Materials Research* **57**: 132–139.

Menke, N.B., Ward, K.R., Witten, T.M., Bonchev, D.G. & Diegelmann, R.F. (2007) Impaired wound healing. *Clinics in Dermatology* **25**: 19–25.

Mundy, G., Garrett, R., Harris, S., Chan, J., Chen, D., Rossini, G., Boyce, B., Zhao, M. & Gutierrez, G. (1999) Stimulation of bone formation in vitro and in rodents by statins. *Science* **286**: 1946–1949.

Nyan, M., Sato, D., Oda, M., Machida, T., Kobayashi, H., Nakamura, T. & Kasugai, S. (2007) Bone formation with the combination of simvastatin and calcium sulfate in critical-sized rat calvarial defect. *Journal of Pharmacological Science* **104**: 384–386.

Ohnaka, K., Shimoda, S., Nawata, H., Shimokawa, H., Kaibuchi, K., Iwamoto, Y. & Takayanagi, R. (2001) Pitavastatin enhanced BMP-2 and osteocalcin expression by inhibition of Rho-associated kinase in human osteoblasts. *Biochemical and Biophysical Research Communications* **287**: 337–342.

Ozec, I., Kilic, E., Gumus, C. & Goze, F. (2007) Effect of local simvastatin application on mandibular defects. *Journal of Craniofacial Surgery* **18**: 546–550.

Saito, A., Suzuki, Y., Kitamura, M., Ogata, S., Yoshihara, Y., Masuda, S., Ohtsuki, C. & Tanihara, M. (2006) Repair of 20-mm long rabbit radial bone defects using BMP-derived peptide combined with an α-tricalcium phosphate scaffold. *Journal of Biomedical Materials Research* **77A**: 700–706.

Sato, D., Nishimura, K., Ishioka, T., Kondo, H., Kuroda, S. & Kasugai, S. (2005) Local application of simvastatin to rat incisor socket: carrier-dependent effect on bone augmentation. *Journal of Oral Tissue Engineering* **2**: 81–85.

Skoglund, B., Forslund, C. & Aspenberg, P. (2002) Simvastatin improves fracture healing in mice. *Journal of Bone and Mineral Research* **17**: 2004–2008.

Song, C., Guo, Z., Ma, Q., Chen, Z., Liu, Z., Jia, H. & Dang, G. (2003) Simvastatin induces osteoblastic differentiation and inhibits adipocytic differentiation in mouse bone marrow stromal cells. *Biochemical and Biophysical Research Communications* **308**: 458–462.

Stein, D., Lee, Y., Schmid, M.J., Killpack, B., Genrich, M.A., Narayana, N., Mark, D.B., Cullen, D.M. & Reinhardt, R.A. (2005) Local simvastatin effects on mandibular bone growth and inflammation. *Journal of Periodontology* **76**: 1861–1870.

Sugiyama, M., Kodama, T., Konisihi, K., Abe, K., Asami, S. & Oikawa, S. (2000) Compactin and simvastatin, but not pravastatin, induce bone morphogentic-2 in human osteosarcoma cells. *Biochemical Biophysical Research Communications* **271**: 688–692.

Sugiyama, T., Nakagawa, T., Sato, C., Fujii, T., Mine, K., Shimizu, K., Murata, T. & Tagawa, T. (2007) Subcutaneous administration of lactone form of simvastatin stimulates ectopic osteoinduction by rhMBP-2. *Oral Diseases* **13**: 228–233.

Szpaderska, A. & DiPietro, L.A. (2005) Inflammation in surgical wound healing: friend or foe? *Surgery* **137**: 571–573.

Thylin, M.R., McConnell, J.C., Schmid, M.J., Reckling, R.R., Ojha, J., Bhattacharyya, I., Marx, D.V. & Reinhardt, R.A. (2002) Effects of statin gels on murine calvarial bone. *Journal of Periodontology* **73**: 1141–1148.

Weitz-Schmidt, G. (2002) Statins as anti-inflammatory agents. *Trends in Pharmacological Sciences* **23**: 482–487.

Wikesjo, U.M.E. & Selvig, K.A. (1999) Periodontal wound healing and regeneration. *Periodontology 2000* **19**: 21–39.

Wiltfang, J., Merten, H.A., Schlegel, K.A., Schultze-Mosgau, S., Kloss, F.R., Rupprecht, S. & Kessler, P. (2002) Degradation characteristics of α and β tri-calcium-phosphate (TCP) in minipigs. *Journal of Biomedical Materials Research* **63**: 115–121.

Wong, R.W.K. & Rabie, A.B.M. (2003) Statin collagen grafts used to repair bone defects in the parietal bone of rabbits. *British Journal of Oral and Maxillofacial Surgery* **41**: 244–248.

Wong, R.W.K. & Rabie, A.B.M. (2005a) Histologic and ultrastructural study on statin graft in rabbit skulls. *Journal of Oral and Maxillofacial Surgery* **63**: 1515–1521.

Wong, R.W.K. & Rabie, A.B.M. (2005b) Early healing pattern of statin-induced osteogenesis. *British Journal of Oral and Maxillofacial Surgery* **43**: 46–50.

Yan, W.Z., Zhou, D.L., Yin, S.Y., Yin, G.F., Gao, L.D. & Zhang, Y. (2004) Osteogenesis capacity of a novel BMP/α-TCP bioactive composite bone cement. *Journal of Wuhan University of Technology – Materials Science* **19**: 30–34.

Ziegler, J., Mayr-Wohlfart, U., Kessler, S., Breitig, D. & Gunther, K.P. (2002) Adsorption and release properties of growth factors from biodegradable implants. *Journal of Biomedical Materials Research* **59**: 422–428.

Effects of Cholesterol-Bearing Pullulan (CHP)-Nanogels in Combination with Prostaglandin E1 on Wound Healing

Hiroshi Kobayashi,[1] Osamu Katakura,[1] Nobuyuki Morimoto,[2] Kazunari Akiyoshi,[2,3] Shohei Kasugai[1,3]

[1] Oral Implantology and Regenerative Dental Medicine, Tokyo Medical and Dental University, Bunkyo-ku, Tokyo 113-8549, Japan

[2] Institute of Biomaterials and Bioengineering, Tokyo Medical and Dental University, Chiyoda-ku, Tokyo 101-0062, Japan

[3] Global Center of Excellence (GCOE) Program, International Research Center for Molecular Science in Tooth and Bone Diseases, Tokyo, Japan

Received 12 February 2008; revised 11 November 2008; accepted 18 November 2008
Published online 16 April 2009 in Wiley InterScience (www.interscience.wiley.com). DOI: 10.1002/jbm.b.31373

Abstract: The cholesterol-bearing pullulan (CHP)-nanogels are able to trap hydrophobic drugs or proteins inside the nanogels, which is potential in application to drug delivery system and tissue engineering. On the other hand, prostaglandin E1 (PGE1) plays important roles in wound healing and PGE1 ointment has been clinically used to treat chronic skin ulcers and wounds. The purpose of this study is to evaluate effects of CHP nanogels in combination with prostaglandin E1 on wound healing in full thickness skin defect model. A square skin defect (1×1 cm^2) of full thickness was created on the dorsal of Wistar rats. The wound was treated with CHP nanogels without PGE1 (CHP group) or CHP nanogels containing with PGE1 (CHP/PGE1 group) or PGE1 ointment (PGE1 ointment group). In both CHP/PGE1 and PGE1 ointment groups, ~6 μg of PGE1 was applied to each wound. In the control group, the wound was untreated. The wound was evaluated in measuring wound area and histologically. In CHP/PGE1 group, the rate of wound size reduction was significantly higher than the ones of other groups. Histologically, CHP/PGE1 promoted neoepithelialization, neovascularization, and wound closure compared to the other treatments. These results suggest that CHP in combination with PGE1 can promote wound healing, which confirms the efficiency of CHP nanogels-based drug delivery system. © 2009 Wiley Periodicals, Inc. J Biomed Mater Res Part B: Appl Biomater 91B: 55–60, 2009

Keywords: drug delivery system; nanogel; cholesterol-bearing pullulan; prostaglandin E1; wound healing

INTRODUCTION

Wound healing in the skin is a complex biological process in which numerous types of cells, cytokines, growth factors, proteases, and extracellular matrix components play roles. Enhanced epidermal healing in a moist wound environment was demonstrated by Winter in 1962.[1] Furthermore, Vogt et al. reported that a moist or wet healing environment resulted in less necrosis and faster and better quality of healing in the formation of newly regenerated epidermis.[2] Thus, a moist environment is known to accelerate wound re-epithelialization. The ideal wound dressing is biocompatible, protecting the wound from bacterial infection, preventing excessive fluid loss and maintaining a moist healing environment.[3] Currently, various materials, such as gelatin, collagen, polyurethane, and polyethylene are clinically used for wound dressing. Although these wound dressing materials are effective, a wound dressing material, which promotes wound healing more effectively, is strongly required because tremendous number of patients suffer from unhealed wounds, which accompany infection in most cases.

Cholesterol-bearing pullulan (CHP) form nanometer-sized hydrogel (nanogel) by self-assembly in water.[4] The CHP nanogels have multihydrophobic domains consisting of several cholesteryl groups in pullulan.[5] Therefore, CHP nanogels can trap hydrophobic drugs and proteins inside the nanogels and the complex has been applied as drug carriers.[6–8] In our previous reports, PGE2 was trapped in CHP nanogels and injected on to the calvarias of mice, which enhanced local bone formation without any visible side effect.[9] In the case of semi dilute condition of CHP nanogels, physically cross-linked hydrogel is obtained.[10] Using this property, we developed paste (hydrogel) type CHP-nanogels/PGE1 complex.

The biological functions of prostaglandins (PGs) have been widely studied. Prostaglandin E1 (PGE1) is a metabo-

Correspondence to: H. Kobayashi (e-mail: hiro.irm@tmd.ac.jp)

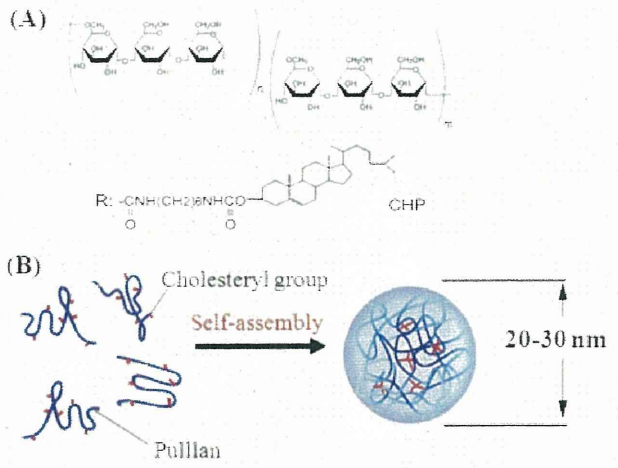

Figure 1. Self-assembly of CHP nanogel and crosslinking based nanogel spheres. (A) Chemical structure of CHP. (B) Formation of nanogel by self-assembly of CHP. [Color figure can be viewed in the online issue, which is available at www.interscience.wiley.com.]

lite of the polyunsaturated dihomogamma-linoleic acid. PGE1 exerts vasodilation and anti-platelet aggregation and it also promotes proliferation of both keratinocytes and fibroblasts.[11] Thus, it has been clinically used to treat burn wounds and various vascular disorders, especially arterial occlusive ischemia. It has been reported that topical application of PGE1 ointment to chronic skin ulcers is effective.[12,13] We speculated that CHP nanogels would be useful as PGE1 carrier for wound treatment. The purpose of this study was to evaluate the effects of CHP nanogels containing prostaglandin E1 *in vivo* full thickness skin defect model.

MATERIALS AND METHODS

Pullulan was substituted with 1.1 cholesterol moieties per 100 anhydrous glucoside units (Figure 1). Cholesterol-bearing pullulan (CHP) was synthesized as previously reported.[4,6–8]

Preparation of CHP Nanogels Containing PGE1

First, CHP nanogels suspension in PBS (pH 7.5, 40 mg/mL) was prepared. PGE1 (Wako Pure Chemical Industries, Ltd. Osaka, Japan) was added directly to the CHP nanogels suspension and mixed by stirring in the dark at room temperature overnight. The final concentration of CHP/PGE1 was 30 μg/mL. The CHP nanogels/PGE1 complex was obtained as paste and it was stored at 4°C.

Experimental Animals

Forty male Wistar rats (7-weeks old; Sankyo Labo Service Corporation; Tokyo, Japan) were used. Each rat was individually kept in a separate cage to avoid an additional wound by the other rats. They were given free access to food and water. The Committee of Animal Experiments of Tokyo Medical and Dental University approved this experiment.

Experimental Model

The rats weighing ~260 g were anesthetized with an intramuscular injection of ketamine (2 mg/kg body weight) and xylazine (0.25 mg/kg body weight) before the surgery. The dorsal skin was shaved with electric clippers and disinfected with 70% ethanol. A full-thickness square surgical wound, 1×1 cm^2 in size, was prepared on the dorsal skin of each rat. The animals were divided into four groups: the first group was untreated (control group), the second group was applied with CHP nanogels only (CHP group), the third group was applied with CHP nanogels containing PGE1 (CHP/PGE1 group), the fourth group was applied with PGE1 ointment (Ono Pharmaceutical Co. Ltd., Osaka, Japan) (PGE1 ointment group). In both CHP/PGE1 and PGE1 ointment groups, 6 μg of PGE1 was approximately applied to each wound. Then, all wounds including the ones in the control group were covered with polyurethane film (Cathereep^{R}, Nichiban Co. Ltd., Tokyo, Japan), over which sterile gauze was layered, and all layers were fixed with elastic adhesive bandage (Elastpore^{R}, Nichiban Co. Ltd., Tokyo, Japan) and sutures. This wound coverage was schematically presented in Figure 2. The above applications to the wounds were performed at the time of wound creation. For the following wound reduction measurement and histological evaluation, the dressing material of each rat was not removed until the time point of observation. However, exceptionally, for taking time-sequential photographic images from one animal of each group, the dressing material was temporally removed and immediately returned back after taking a photo. It is likely that this procedure did not

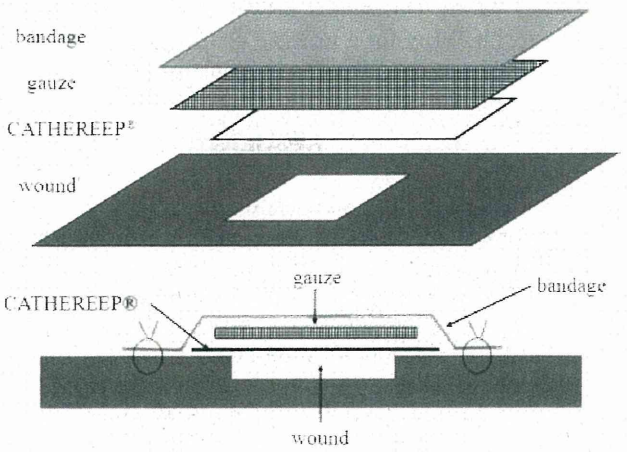

Figure 2. Schematic figure of wound dressing layers in this study.

affect wound healing extensively because the damage of the wound bed was not visually observed during this procedure.

During the experiment, animals were kept in separate cages. The wound together with a ruler was photographed to measure the wound area on day 0, 5, 7, 10, and 14 days after the surgery. In the wound reduction measurements, the photographs were firstly taken and the measurements in the unlabelled photographs were performed. The wound area was measured with an image analysis software (Scion Image). Wound size reduction was calculated by the following numerical formulas:

Wound size reduction (%) = (the original wound area − the wound area on day 5, 7, 10, and 14 day after the surgery) × 100/the original wound area.

Histology

The animals were sacrificed under chloroform anesthesia at 1 and 2 weeks after the surgery. The wounds and their surrounding tissue were excised and then fixed in 10% neutralized-formalin solution. The specimens were dehydrated in ethanol, embedded in paraffin wax and sectioned. The sections were stained with hematoxylin and eosin. For wound re-epithelialization measurement, the photographs were first taken and the measurements in the unlabelled photographs were performed. Percentage of wound re-epithelialization was determined by histomorphometrical analysis. The length of newly generated epithelium across the surface of the wound was determined as the sum of the new epidermis growing from the right and left margins of the wound. This length was expressed as a percentage of initial entire wound length.

Rate of re-epithelialization (%) = (the original wound length − the length of unepithelialized tissues on day 7 and 14 after the surgery) × 100/the original wound length.

Statistical Analyses

All data were presented as the mean ± standard error of mean (SEM). Differences between the groups were examined with Tukey for a multiple comparison test. A value of $p < 0.05$ was considered to be statistically significant.

RESULTS

The images of the wounds of all groups at 0, 7, and 14 days were presented in Figure 3. We measured the wound area at 0, 5, 7, 10, and 14 days and calculated wound size reduction. Figure 4 shows the wound size reduction of all groups at 5, 7, 10, and 14 days. Obviously, wound size reduction of CHP/PGE1 group was superior to the ones of other three groups at every time point. Furthermore, wound size reduction of the CHP group was higher than that of the control groups at all four time points. Interestingly, wound size reduction of CHP group was higher than that of the PGE1 ointment group at 5 and 14 days.

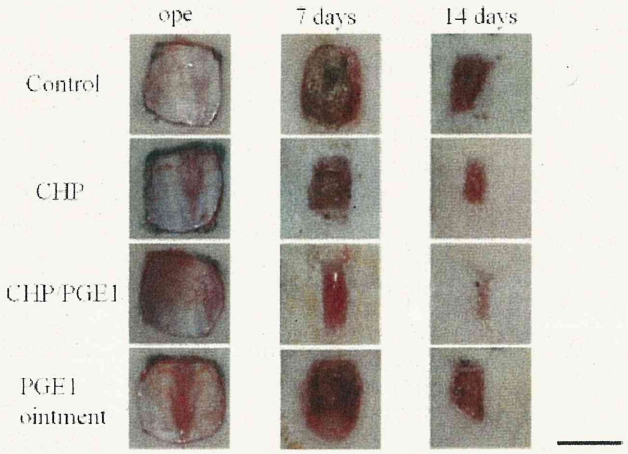

Figure 3. Photographic result of wounds covered with CHP, CHP/PGE1, and PGE1 ointment compared with untreated (control). Black line: 10 mm. [Color figure can be viewed in the online issue, which is available at www.interscience.wiley.com.]

Figure 5 shows the rate of wound re-epithelialization of all groups at 7 and 14 days. At 7 days, the rate of re-epithelialization of CHP/PGE1 group was higher than those of other three groups. At 14 days, the rate of re-epithelialization of CHP/PGE1 group was significantly higher than those of the control and PGE1 ointment groups. At 14 days in CHP group re-epithelialization was more prominent than those of the control and PGE1 ointment groups.

To evaluate the quality of the regenerated tissues, we performed hematoxylin-eosin (H-E) staining of the histological sections. Figure 6 shows the histological images of the wound tissues of all groups at 7 days. In the control group [Figure 6(A)], approximately one-third of the wound was covered with epithelium; however, the other wound surface was covered by necrotic tissue under which numerous neutrophils and macrophages were observed. The granulation tissue, which included numerous inflammatory cells, was evident in the dermis, and a scab was formed over the wound. In the CHP group [Figure 6(B)], epithelium covered approximately a half of the wound and numerous inflammatory cells were similarly observed in dermis, where more capillaries were observed compared to the control group. In the CHP/PGE1 group [Figure 6(C)], the neoepithelium from the edge of the wound was much longer than that of the other groups. In the dermis, there were fewer neutrophils and more capillaries than the control and PGE1 ointment groups. In the PGE1 ointment group [Figure 6(D)], approximately two-fifth of the wound was covered with new epithelium and numerous inflammatory cells were seen in the dermis.

Figure 7 shows the histological images of the wound tissues of all groups at 14 days. In the control group [Figure 7(A)], the wound was not completely covered with epithelium and inflammatory cells still existed in the center of the wound. In the CHP group [Figure 7(B)], the wound was almost completely covered with epithelium and there